cell lines and/or human melanoma samples, is required to obtain conclusive evidence.

In conclusion, the robust finding of our study suggests that Epac may serve as a target molecule in melanoma cancer thereby inhibiting melanoma metastasis, even though we do not yet know whether Epac similarly regulates HS signaling in other cancer cell types.

ACKNOWLEDGMENTS

We thank Lauren Danridge for critical reading of the manuscript.

GRANTS

This study was supported in part by grants from the Japan Space Forum, the Japanese Ministry of Education, Culture, Sports, Science, and Technology, and the Takeda Science Foundation and National Institutes of Health Grants GM-067773 and HL-059139 (to Y. Ishikawa), and the American Heart Association (SDG 0835596D) and the Foundation of UMDNJ (K. Iwatsubo).

REFERENCES

1. **Araki E, Momota Y, Togo T, Tanioka M, Hozumi K, Nomizu M, Miyachi Y, Utani A.** Clustering of Syndecan-4 and integrin β1 by iaminin α3 chain-derived peptide promotes keratinocyte migration. *Mol Biol Cell* 20: 3012–3024, 2009.
2. **Bellahcene A, Castronovo V, Ogbureke KU, Fisher LW, Fedarko NS.** Small integrin-binding ligand N-linked glycoproteins (SIBLINGs): multifunctional proteins in cancer. *Nat Rev Cancer* 8: 212–226, 2008.
3. **Benoist F and Grand-Perret T.** Cotranslational degradation of apolipoprotein B100 by the proteasome is prevented by microsomal triglyceride transfer protein synchronized translation studies on HepG2 cells treated with an inhibitor of microsomal triglyceride transfer protein. *J Biol Chem* 272: 20435–20442, 1997.
4. **Bernfield M, Gotte M, Park PW, Reizes O, Fitzgerald ML, Lincecum J, Zako M.** Functions of cell surface heparan sulfate proteoglycans. *Ann Rev Biochem* 68: 729–777, 1999.
5. **Berwick M, Wiggins C.** The current epidemiology of cutaneous malignant melanoma. *Front Biosci* 11: 1244–1254, 2006.
6. **Bos JL.** Epac proteins: multi-purpose cAMP targets. *Trends Biochem Sci* 31: 680–686, 2006.
7. **Brennesvik EO, Ktori C, Ruzzin J, Jebens E, Shepherd PR, Jensen J.** Adrenaline potentiates insulin-stimulated PKB activation via cAMP and Epac: implications for cross talk between insulin and adrenaline. *Cell Signal* 17: 1551–1559, 2005.
8. **Brockstedt U, Dobra K, Nurminen M, Hjerpe A.** Immunoreactivity to cell surface syndecans in cytoplasm and nucleus: tubulin-dependent rearrangements. *Exp Cell Res* 274: 235–245, 2002.
9. **Byers HR, Etoh T, Doherty JR, Sober AJ, Mihm MC Jr.** Cell migration and actin organization in cultured human primary, recurrent cutaneous and metastatic melanoma. Time-lapse and image analysis. *Am J Pathol* 139: 423–435, 1991.
10. **Choi S, Kim Y, Park H, Han IO, Chung E, Lee SY, Kim YB, Lee JW, Oh ES, Yi JY.** Syndecan-2 overexpression regulates adhesion and migration through cooperation with integrin alpha2. *Biochem Biophys Res Commun* 384: 231–235, 2009.
11. **Claffey KP, Brown LF, del Aguila LF, Tognazzi K, Yeo KT, Manseau EJ, Dvorak HF.** Expression of vascular permeability factor/vascular endothelial growth factor by melanoma cells increases tumor growth, angiogenesis, and experimental metastasis. *Cancer Res* 56: 172–181, 1996.
12. **de Rooij J, Zwartkruis FJ, Verheijen MH, Cool RH, Nijman SM, Wittinghofer A, Bos JL.** Epac is a Rap1 guanine-nucleotide-exchange factor directly activated by cyclic AMP. *Nature* 396: 474–477, 1998.
13. **Ethell IM, Yamaguchi Y.** Cell surface heparan sulfate proteoglycan syndecan-2 induces the maturation of dendritic spines in rat hippocampal neurons. *J Cell Biol* 144: 575–586, 1999.
14. **Fjeldstad K, Kolset SO.** Decreasing the metastatic potential in cancers–targeting the heparan sulfate proteoglycans. *Curr Drug Targets* 6: 665–682, 2005.
15. **Galbraith JA, Gallant PE.** Axonal transport of tubulin and actin. *J Neurocytol* 29: 889–911, 2000.
16. **Gao L, Feng Y, Bowers R, Becker-Hapak M, Gardner J, Council L, Linette G, Zhao H, Cornelius LA.** Ras-associated protein-1 regulates extracellular signal-regulated kinase activation and migration in melanoma cells: two processes important to melanoma tumorigenesis and metastasis. *Cancer Res* 66: 7880–7888, 2006.
17. **Hadjidemetriou S, Toomre D, Duncan J.** Motion tracking of the outer tips of microtubules. *Med Image Anal* 2008.
18. **Head BP, Patel HH, Roth DM, Murray F, Swaney JS, Niesman IR, Farquhar MG, Insel PA.** Microtubules and actin microfilaments regulate lipid raft/caveolae localization of adenylyl cyclase signaling components. *J Biol Chem* 281: 26391–26399, 2006.
19. **Iozzo RV.** Series Introduction: Heparan sulfate proteoglycans: intricate molecules with intriguing functions. *J Clin Invest* 108: 165–167, 2001.
20. **Iwatsubo K, Minamisawa S, Tsunematsu T, Nakagome M, Toya Y, Tomlinson JE, Umemura S, Scarborough RM, Levy DE, Ishikawa Y.** Direct inhibition of type 5 adenylyl cyclase prevents myocardial apoptosis without functional deterioration. *J Biol Chem* 279: 40938–40945, 2004.
21. **Iwatsubo K, Suzuki S, Li C, Tsunematsu T, Nakamura F, Okumura S, Sato M, Minamisawa S, Toya Y, Umemura S, Ishikawa Y.** Dopamine induces apoptosis in young, but not in neonatal, neurons via Ca^{2+}-dependent signal. *Am J Physiol Cell Physiol* 293: C1498–C1508, 2007.
22. **Jing H, Yen JH, Ganea D.** A novel signaling pathway mediates the inhibition of CCL3/4 expression by prostaglandin E2. *J Biol Chem* 279: 55176–55186, 2004.
23. **Kawabe J, Okumura S, Lee MC, Sadoshima J, Ishikawa Y.** Translocation of caveolin regulates stretch-induced ERK activity in vascular smooth muscle cells. *Am J Physiol Heart Circ Physiol* 286: H1845–H1852, 2004.
24. **Kopatz I, Remy JS, Behr JP.** A model for non-viral gene delivery: through syndecan adhesion molecules and powered by actin. *J Gene Med* 6: 769–776, 2004.
25. **Krauss K, Altevogt P.** Integrin leukocyte function-associated antigen-1-mediated cell binding can be activated by clustering of membrane rafts. *J Biol Chem* 274: 36921–36927, 1999.
26. **Leitinger B, Hogg N.** The involvement of lipid rafts in the regulation of integrin function. *J Cell Sci* 115: 963–972, 2002.
27. **Lester BR, Greig RG, Buscarino C, Sheppard JR, Corwin SP, Poste G.** cAMP metabolism in B16 melanoma clones during the formation of experimental and spontaneous metastases. *Int J Cancer* 38: 405–411, 1986.
28. **Lorenowicz MJ, van Gils J, de Boer M, Hordijk PL, and Fernandez-Borja M.** Epac1-Rap1 signaling regulates monocyte adhesion and chemotaxis. *J Leukoc Biol* 80: 1542–1552, 2006.
29. **Mei FC, Cheng X.** Interplay between exchange protein directly activated by cAMP (Epac) and microtubule cytoskeleton. *Mol BioSys* 1: 325–331, 2005.
30. **Millan J, Hewlett L, Glyn M, Toomre D, Clark P, Ridley AJ.** Lymphocyte transcellular migration occurs through recruitment of endothelial ICAM-1 to caveola- and F-actin-rich domains. *Nat Cell Biol* 8: 113–123, 2006.
31. **Misra UK, Pizzo SV.** Coordinate regulation of forskolin-induced cellular proliferation in macrophages by protein kinase A/cAMP-response element-binding protein (CREB) and Epac1-Rap1 signaling: effects of silencing CREB gene expression on Akt activation. *J Biol Chem* 280: 38276–38289, 2005.
32. **Nuzzi PA, Senetar MA, Huttenlocher A.** Asymmetric localization of calpain 2 during neutrophil chemotaxis. *Mol Biol Cell* 18: 795–805, 2007.
33. **Ormerod EJ, Hart IR.** Different growth responses to agents which elevate cAMP in human melanoma cell lines of high and low experimental metastatic capacity. *Clin Exp Metast* 7: 85–95, 1989.
34. **Oshikawa J, Otsu K, Toya Y, Tsunematsu T, Hankins R, Kawabe J, Minamisawa S, Umemura S, Hagiwara Y, Ishikawa Y.** Insulin resistance in skeletal muscles of caveolin-3-null mice. *Proc Natl Acad Sci USA* 101: 12670–12675, 2004.
35. **Qiao D, Meyer K, Mundhenke C, Drew SA, Friedl A.** Heparan sulfate proteoglycans as regulators of fibroblast growth factor-2 signaling in brain endothelial cells. Specific role for glypican-1 in glioma angiogenesis. *J Biol Chem* 278: 16045–16053, 2003.
36. **Raats CJI, Bakker MAH, van den Born J, Berden JHM.** Hydroxyl radicals depolymerize glomerular heparan sulfate in vitro and in experimental nephrotic syndrome. *J Biol Chem* 272: 26734–26741, 1997.
37. **Rickard A, Portell C, Siegal J, Goeckeler Z, Lagunoff D.** Measurement of the motility of endothelial cells in confluent monolayers. *Microcirculation* 10: 193–203, 2003.
38. **Thomas LA, Yamada KM.** Contact stimulation of cell migration. *J Cell Sci* 103: 1211–1214, 1992.

39. **Tkachenko E, Elfenbein A, Tirziu D, Simons M.** Syndecan-4 clustering induces cell migration in a PDZ-dependent manner. *Circ Res* 98: 1398–1404, 2006.
40. **Tkachenko E, Simons M.** Clustering induces redistribution of syndecan-4 core protein into raft membrane domains. *J Biol Chem* 277: 19946–19951, 2002.
41. **Ulucan C, Wang X, Baljinnyam E, Bai Y, Okumura S, Sato M, Minamisawa S, Hirotani S, Ishikawa Y.** Developmental changes in gene expression of Epac and its upregulation in myocardial hypertrophy. *Am J Physiol Heart Circ Physiol* 293: H1662–H1672, 2007.
42. **Williams TM, Lisanti MP.** The Caveolin genes: from cell biology to medicine. *Ann Med* 36: 584–595, 2004.
43. **Wolter KG, Verhaegen M, Fernandez Y, Nikolovska-Coleska Z, Riblett M, de la Vega CM, Wang S, Soengas MS.** Therapeutic window for melanoma treatment provided by selective effects of the proteasome on Bcl-2 proteins. *Cell Death Differ* 14: 1605–1616, 2007.
44. **Yokoyama U, Minamisawa S, Quan H, Ghatak S, Akaike T, Segi-Nishida E, Iwasaki S, Iwamoto M, Misra S, Tamura K, Hori H, Yokota S, Toole BP, Sugimoto Y, Ishikawa Y.** Chronic activation of the prostaglandin receptor EP4 promotes hyaluronan-mediated neointimal formation in the ductus arteriosus. *J Clin Invest* 116: 3026–3034, 2006.
45. **Yoneda A, Couchman JR.** Regulation of cytoskeletal organization by syndecan transmembrane proteoglycans. *Matrix Biol* 22: 25–33, 2003.
46. **Yu HR, Schultz RM.** Relationship between secreted urokinase plasminogen activator activity and metastatic potential in murine B16 cells transfected with human urokinase sense and antisense genes. *Cancer Res* 50: 7623–7633, 1990.
47. **Zhang L, Schwartz JJ, Miller J, Liu J, Fritze LMS, Shworak NW, Rosenberg RD.** The retinoic acid and cAMP-dependent up-regulation of 3-*O*-sulfotransferase-1 leads to a dramatic augmentation of anticoagulantly active heparan sulfate biosynthesis in F9 embryonal carcinoma Cells. *J Biol Chem* 273: 27998–28003, 1998.
48. **Zhou FQ, Snider Cell biology WD.** GSK-3beta and microtubule assembly in axons. *Science* 308: 211–214, 2005.
49. **Zumbrunn J, Kinoshita K, Hyman AA, Nathke IS.** Binding of the adenomatous polyposis coli protein to microtubules increases microtubule stability and is regulated by GSK3 beta phosphorylation. *Curr Biol* 11: 44–49, 2001.

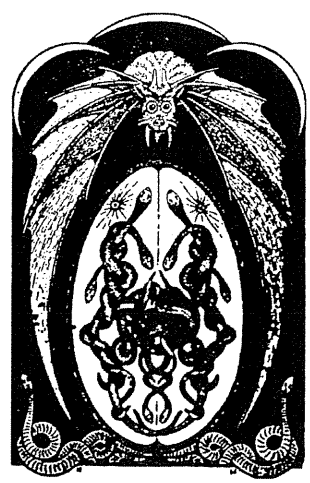

THE JOURNAL OF BIOLOGICAL CHEMISTRY VOL. 284, NO. 45, pp. 31431–31440, November 6, 2009

Activator of G Protein Signaling 8 (AGS8) Is Required for Hypoxia-induced Apoptosis of Cardiomyocytes

ROLE OF Gβγ AND CONNEXIN 43 (CX43)[*][S]

Received for publication, April 30, 2009, and in revised form, August 13, 2009 Published, JBC Papers in Press, September 1, 2009, DOI 10.1074/jbc.M109.014068

Motohiko Sato[‡1,2], **Qibin Jiao**[‡1], **Takashi Honda**[‡], **Reiko Kurotani**[‡], **Eiji Toyota**[§], **Satoshi Okumura**[‡], **Tatsuo Takeya**[¶], **Susumu Minamisawa**[‖], **Stephen M. Lanier**[**], **and Yoshihiro Ishikawa**[‡3]

From the [‡]*Cardiovascular Research Institute, Yokohama City University School of Medicine, Fukuura, Yokohama 236-0004, Japan, the* [§]*Department of of Cardiology, Kawasaki Medical School, Kurashiki 701-0192, Japan, the* [¶]*Graduate School of Biological Sciences, Nara Institute of Science and Technology, Nara 630-0101, Japan, the* [‖]*Department of Life Science and Medical Bioscience, Waseda University, Tokyo 162-8480, Japan, and the* [**]*Department of Pharmacology, Medical University of South Carolina, Charleston, South Carolina 29425*

Ischemic injury of the heart is associated with activation of multiple signal transduction systems including the heterotrimeric G-protein system. Here, we report a role of the ischemia-inducible regulator of Gβγ subunit, AGS8, in survival of cardiomyocytes under hypoxia. Cultured rat neonatal cardiomyocytes (NCM) were exposed to hypoxia or hypoxia/reoxygenation following transfection of AGS8siRNA or pcDNA::AGS8. Hypoxia-induced apoptosis of NCM was completely blocked by AGS8siRNA, whereas overexpression of AGS8 increased apoptosis. AGS8 formed complexes with G-proteins and channel protein connexin 43 (CX43), which regulates the permeability of small molecules under hypoxic stress. AGS8 initiated CX43 phosphorylation in a Gβγ-dependent manner by providing a scaffold composed of Gβγ and CX43. AGS8siRNA blocked internalization of CX43 following exposure of NCM to repetitive hypoxia; however it did not influence epidermal growth factor-mediated internalization of CX43. The decreased dye flux through CX43 that occurred with hypoxic stress was also prevented by AGS8siRNA. Interestingly, the Gβγ inhibitor Gallein mimicked the effect of AGS8 knockdown on both the CX43 internalization and the changes in cell permeability elicited by hypoxic stress. These data indicate that AGS8 is required for hypoxia-induced apoptosis of NCM, and that AGS8-Gβγ signal input increased the sensitivity of cells to hypoxic stress by influencing CX43 regulation and associated cell permeability. Under hypoxic stress, this unrecognized response program plays a critical role in the fate of NCM.

G-protein-coupled receptors (GPCRs)[4] are signaling proteins on the cell surface responsible for mediating various ligands, such as hormones and neurotransmitters. Activation of cell surface GPCRs initiates nucleotide exchange on Gα subunits, which leads to a conformational change of Gαβγ and subsequent transduction of signals to various intracellular effector molecules (1–3). In addition to such established signaling pathways, recent studies indicate the existence of a novel class of regulatory proteins for heterotrimeric G-proteins. These regulatory proteins may provide alternative signal processing via Gαβγ, Gα, or Gβγ subunits distinct from typical GPCR pathways, and identifying these mechanisms may uncover unrecognized roles of G-proteins beyond simple transducers of signals from GPCRs (4–6).

During the alteration of signaling pathways in disease states, such regulatory proteins may be involved in adaptation programs of cells to maintain homeostasis (7–11). Genetic modification of regulatory proteins for G-proteins leads to the development of cardiovascular dysfunction in mice including hypertension, maladaptive response to pressure overload, or altered baroreceptor reflex (9, 12, 13). Thus, such regulatory accessory proteins may be involved in the development of disease via either regulating GPCR-initiated signals or by undefined, alternative G-protein signaling pathways operating independent of the receptor.

In our efforts to adaptation-specific signal regulators for G-protein systems, we identified a novel receptor-independent G-protein activator, activator of G-protein signaling 8 (AGS8), from a cDNA library of rat hearts subjected to repetitive transient ischemia with the development of collateral vessels (8). Initial observations indicated that AGS8 was up-regulated in cardiomyocytes in response to transient ischemia and hypoxia.

* This work was supported, in whole or in part, by National Institutes of Health Grants NS24821 and DA025896 (to S. M. L.). This work was also supported by Grants-in-Aid for Scientific Research (C) 18599006 and 20590212 (to M. S.) and 18057018 and 193902217 (to Y. I.), the Yokohama Foundation for Advancement of Medical Science (to M. S.), grants from the Strategic Research Project K18017 and K19021 of Yokohama City University, Japan (to M. S.), and a grant from the Takeda Science Foundation (to Y. I.).

[S] The on-line version of this article (available at http://www.jbc.org) contains supplemental materials and Figs. S1 and S2 .

[1] Both authors contributed equally to the studies presented in this report.

[2] Recipient of grants from the Takeda Science Foundation, NOVARTIS Foundation (Japan) for the Promotion of Science, Mitsubishi Pharma Research Foundation, The Ichiro Kanehara Foundation, and Mochida Memorial Foundation for Medical and Pharmaceutical Research. To whom correspondence may be addressed: Cardiovascular Research Institute, Yokohama City University School of Medicine, 3-9 Fukuura, Kanazawa-Ku, Yokohama 236-0004, Japan. Fax: 1-81-45-788-1470; E-mail: motosato@yokohama-cu.ac.jp.

[3] To whom correspondence may be addressed: Fax: 1-81-45-788-1470; E-mail: yishikaw@med.yokohama-cu.ac.jp.

[4] The abbreviations used are: GPCR, G-protein-coupled receptor; AGS8, activator of G protein signaling 8; CX43, connexin 43; NCM, neonatal cardiomyocyte; siRNA, small interfering RNA; LY, lucifer yellow; EGF, epidermal growth factor; GST, glutathione *S*-transferase; TUNEL, terminal deoxynucleotidyltransferase-mediated dUTP nick end-labeling; DAPI, 4′,6-diamidino-2-phenylindole; analysis of variance.

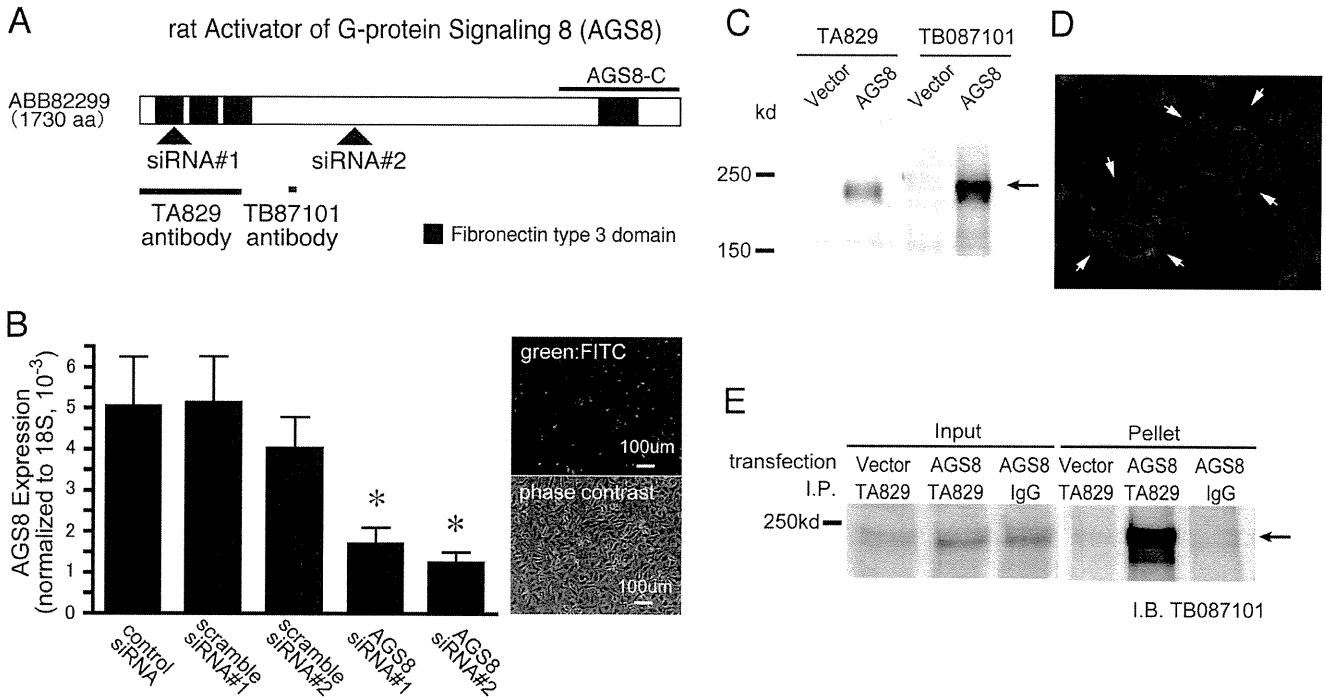

FIGURE 1. **The schematic diagram of AGS8 and the characterization of AGS8siRNA or AGS8 antibodies.** *A*, schematic diagram of AGS8 showing target regions of siRNAs and epitopes of antibodies. *Arrowheads* indicate the target for each siRNA for AGS8. *Solid bars* indicate the epitope of each AGS8 antibodies. AGS8-C, 372 amino acid of the C-terminal region of AGS8. *B*, suppression of AGS8 by siRNA in cultured cardiomyocytes. Neonatal cardiomyocytes were transfected with 50 nM siRNAs for AGS8 as well as control siRNAs. Control siRNA is the universal negative siRNA control designed to minimize sequence homology to any known vertebrate transcript (Stealth RNAi Negative Control). 48 h after transfection, the level of mRNA of AGS8 was analyzed by real-time PCR. Transfection efficiency of siRNA was estimated 70–80% using FITC-labeled dsRNA (Block It Fluorescent Oligo, Invitrogen) (*right panel*). *, $p < 0.05$ *versus* negative siRNA. $n = 8$ from four independent experiments. *C*, detection of expressed AGS8 by AGS antibody (TA829). COS7 cells were transfected with pcDNAHis (4 μg/35-mm dish) or pcDNAHis::AGS8 (4 μg/35-mm dish). After 48 h of transfection, cells were solubilized into Laemmli buffer, and 10 μg of cell lysates were subjected to immunoblot. (TA829, 1:1000; TB087101, 1:3000). *D*, immunofluorescence stain of expressed AGS8 in COS7 cells. COS7 cells transfected with pcDNA::AGS8 (4 μg/35-mm dish) were subjected to immunofluorescence stain for AGS8 (TA829, 1:200, *red, arrow*) and nuclei (DAPI, *blue*). *E*, immunoprecipitation of AGS8 from cell lysate. 3 μg of AGS8 antibody (TA829) or rabbit IgG was added to 1 mg of lysate prepared from COS7 cells transfected with pcDNAHis vector (12 μg/dish) or pcDNAHis::AGS8 (12 μg/dish) and incubated 18 h at 4 °C with rotation. The antibody was absorbed to protein G-Sepharose (25 μl of a 50% slurry). The pellets were eluted in 30 μl of 2× Laemmli buffer and subjected to SDS-PAGE. AGS8 was detected by AGS8 antibody (TB087101, 1:1000).

AGS8 directly interacted with G$\beta\gamma$ and regulated G$\beta\gamma$ signaling in cells (8, 14). The induction of AGS8 in tissue and cells suggests that AGS8 may be involved in the adaptation of cardiomyocytes to ischemia, which determines the survival or death of cells.

Here, we report the involvement of AGS8 in cardiomyocyte survival following exposure to hypoxic stresses, and identify protein(s) associated with AGS8 that may regulate cellular events in response to stress. The suppression of AGS8 completely blocked hypoxia-induced apoptosis of cardiomyocytes, indicating that AGS8 is required for hypoxic stress-induced cell death. AGS8 formed complexes with a channel protein connexin 43 (CX43) and regulated its phosphorylation in a G$\beta\gamma$-dependent manner. AGS8siRNA blocked hypoxia-induced internalization of CX43 from the cell-surface that was associated with the altered permeability of molecules flowing through CX43. Interestingly, such AGS8-mediated regulation of CX43 was not observed for receptor-stimulated internalization of CX43 by epidermal growth factor (EGF). Subsequent experiments indicated that the effects of AGS8siRNA were mimicked by a G$\beta\gamma$ signal inhibitor. AGS8-G$\beta\gamma$ may influence the sensitivity of cells to hypoxia via regulating the permeability of CX43 in the membrane. Such undefined regulatory mechanism may play critical roles in the survival of cardiomyocytes.

EXPERIMENTAL PROCEDURES

Materials—Anti-connexin 43 antibody, β-actin antibody, IGEPAL CA-630 were purchased from Sigma. Anti-connexin 43 monoclonal antibody and phospho-connexin 43 (Ser-368) were obtained from Chemicon and Cell Signaling Technology, respectively. Anti-desmoplakin 1&2 antibody and anti-N-cadherin antibody were purchased from PROGEN Biotechnik GmbH (Heidelberg, Germany) and BD Transduction Laboratories, respectively. Anti-Xpress antibody and Lipofectamine 2000 Reagent were purchased from Invitrogen. Anti-Gβ antibody and phospho-connexin 43 (Ser-262) were obtained from Santa Cruz Biotechnology. Rat recombinant epidermal growth factor and Gallein were purchased from Funakosi (Tokyo, Japan) and Calbiochem, respectively. PMH::connexin 43 (rat) was prepared as described previously (15).

Transfection of Small Interfering RNA (siRNA) and Plasmid to Cultured Cardiomyocytes—A double-strand siRNA oligonucleotide to rat AGS8 (DQ256268) was synthesized (Stealth siRNA, Invitrogen) as follows: AGS8 siRNA1 (nt 320–

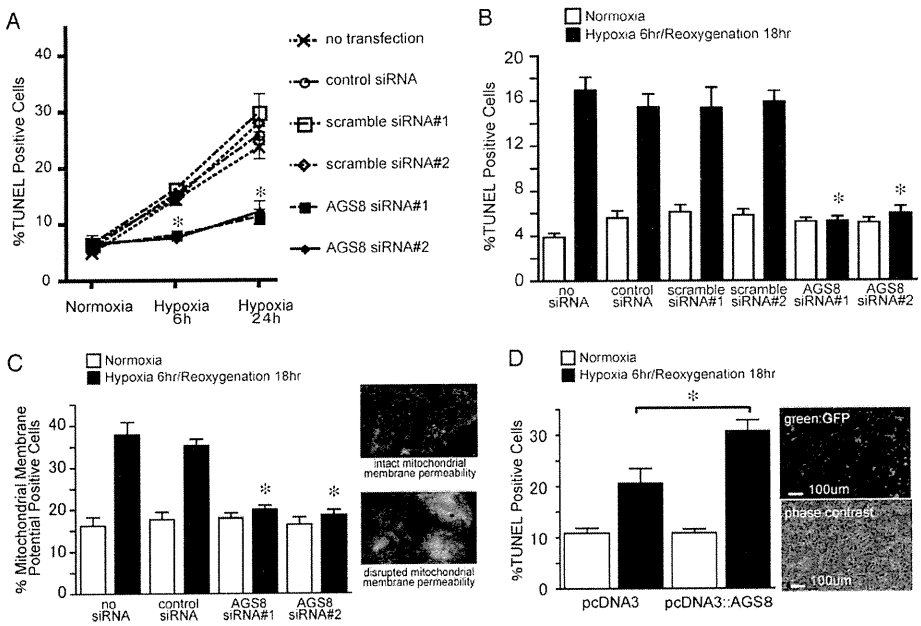

FIGURE 2. **Effect of suppression of AGS8 on apoptosis of cardiomyocytes exposed to hypoxia or hypoxia/reoxygenation.** *A*, effect of suppression of AGS8 on hypoxia-induced apoptosis of cardiomyocytes. Neonatal cardiomyocytes were exposed to hypoxia (1% oxygen) or cultured in normoxia as indicated duration following transfection of siRNA. TUNEL-positive cells were counted from 3000 cells of 10 independent fields in each experiment (magnification, 10 × 20). *, $p < 0.05$ *versus* scramble siRNA at the same condition; $n = 6-7$ of four independent experiments. *B*, effect of suppression of AGS8 on apoptosis of cardiomyocytes following hypoxia/reoxygenation. Neonatal cardiomyocytes were subjected to sequential exposure of 6 h of hypoxia (1% oxygen) followed by 18 h of reoxygenation 48 h after transfection of siRNA. TUNEL-positive cells were counted from 3000 cells of 10 independent fields in each experiment (magnification, 10 × 20). *, $p < 0.05$ *versus* scramble siRNA at the same condition. $n = 8-12$ of five independent experiments. *C*, effect of suppression of AGS8 on apoptosis following hypoxia/reoxygenation. Loss of membrane potential of mitochondria was determined utilizing fluorescence dye staining from 2000 cells of 10 independent fields in each experiment. $n = 6-10$ of five independent experiments. The *right panel* indicates the representative of fluorescence signals determined by this method. *, $p < 0.05$ *versus* scramble siRNA at the same condition. *D*, effect of overexpression of AGS8 on apoptosis of cardiomyocytes following hypoxia/reoxygenation. Neonatal cardiomyocytes were subjected to sequential exposure of 6 h of hypoxia (1% oxygen) followed by 18 h of reoxygenation following transfection of pcDNA3 or pcDNA3::AGS8. TUNEL-positive cells were counted from 3000 cells of 10 independent fields in each experiment (magnification, 10 × 20). Transfection efficiency was estimated at 50–60% using the GFP vector (*right panel*). *, $p < 0.05$. $n = 10$ from five independent experiments.

345, sense: 5′-CCAGAGAUGAGAGAUCGCAUGAAAU-3′), AGS8siRNA2 (nt 2048–2073, sense: 5′-UGGGUCACUUUA-GUUUGAUACGGAA-3′), scramble control from AGS8 siRNA1 (sense: 5′-CCAAGGUGAGAUAGCACGUAAG-AAU-3′), scramble control for AGS8 siRNA2 (sense: 5′-UGG-UCACGAUUGUUUCAUAGUGGAA-3′) (Fig. 1*A*). The conditions and duplex eliciting the most effective reduction in AGS8 were determined in a series of preliminary experiments. Cultured neonatal cardiomyocytes at 1.2×10^5 cell in 24-mm plates were transfected with siRNA using Lipofectamine 2000 according to the manufacturer's instructions. Briefly, RNAi 1 and 2 individually (50 nM) in 10 μl of OPTI-MEM I medium (Invitrogen) and 0.125 μl of Lipofectamine 2000 in 10 μl of OPTI-MEM I media were mixed and then added to the mixture in 24-mm dishes. The transfection efficiency of FITC-labeled oligonucleotide was 70–80% and siRNA for AGS8 did not influence the level of mRNA of β-actin in the condition used (Fig. 1*B*). Negative controls of siRNA for AGS8 were scrambled sequence of siRNA for AGS8 or universal control sequence, which has minimized homology to any known vertebrate transcript with similar GC content (Stealth RNAi Negative Control, Invitrogen). To overexpress AGS8, pcDNA3::AGS8 was transferred to cardiomyocyte utilizing viral envelope system in according to the manufacturer's instructions (GenomOne-Neo, Ishihara Corp. Osaka, Japan). The increase of mRNA of AGS8 was confirmed by real-time PCR following transfection of pcDNA3::AGS8.

Generation of AGS8 Antibody—Antipeptide AGS8 antiserum (TB087101 serum) was generated by immunizing rabbits with the synthetic peptide C-^{612}STSPLSRGWK-DRQDTH-A^{628} following KLH conjugation (Fig. 1*A*). Another AGS8 antiserum (TA829 serum) was generated by immunizing rabbits with a recombinant protein of AGS8 (M1-K330) synthesized as glutathione *S*-transferase (GST) fusion protein in bacteria (Fig. 1*A*). The antiserums were affinity purified and used in subsequent experiments. The antibodies for GST proteins were removed from TA829 by filtration of immune sera through immobilized GST affinity column. Antiserum was characterized by analysis of varying amounts of GST-AGS8 fusion proteins and/or extracts from COS7 cells transfected with pcDNA3::AGS8 to determine optimal conditions for immunoblotting. Purified antibodies (TA829, 0.4 mg/ml; TB087101, 1.0 mg/ml) were used for immunoblotting (TA829, 1:1000; TB087101, 1:1000 to 3000) (Fig. 1*C*), immunostain (TA829, 1:100–200) (Fig. 1*D*) and immunoprecipitation (TA829, 1–3.5 μg per sample) (Fig. 1*E*).

Detection of Apoptosis: In Situ Assay for Apoptosis Detection—*In situ* labeling of fragmented DNA in cardiac myocytes was detected by TACS2 TdT-Blue Label *in Situ* Apoptosis Detection kit (Travigen, Inc., Gaithersburg, MD), that detects DNA breaks in genomic DNA by enzymatic incorporation of biotinylated nucleotides followed by the binding of streptavidin-peroxidase conjugates, according to the manufacturer's instructions. Briefly, myocytes were fixed with 3.7% formaldehyde in phosphate-buffered saline for 10 min and with 70% ethanol for 5 min and then incubated in proteinase K (0.02 mg/ml) at room temperature for 5 min. The cells were incubated with 2% hydrogen peroxide for 5 min and washed with labeling buffer consisting of 50 mM Tris (pH 7.5), 5 mM $MgCl_2$, 60 μM 2-mercaptoethanesulfonic acid, and 0.05% bovine serum albumin, followed by 60 min of incubation at 37 °C in labeling buffer containing 150 μM dATP, 150 μM dGTP, 150 μM dTTP, 5 μM biotinylated dCTP, and 40 units/ml of the Klenow fragment of DNA polymerase I. Untreated myocytes incubated with or without 2 mg/ml DNase in the labeling buffer were used as positive or

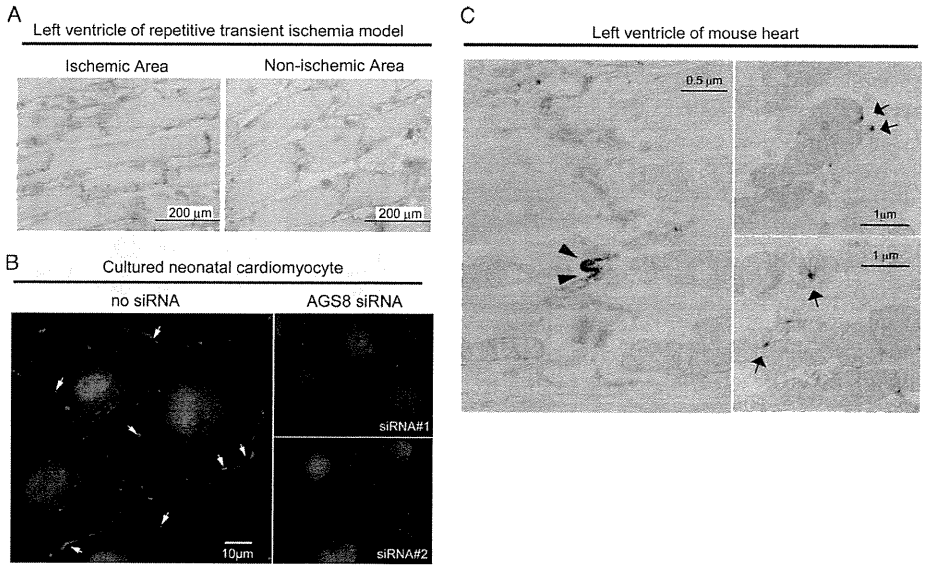

FIGURE 3. **Subcellular distribution of AGS8.** *A*, immunohistochemical staining for AGS8 (TA829, 1:200) of ischemic area (*left*) or non-ischemic area (*right*) of the left ventricle of repetitive transient ischemia model of rat prepared as described previously (8, 18). Frozen section (8 μm) of the rat heart was subjected to immunohistochemical stain as described under supplemental data. *B*, immunofluorescence stain for AGS8 (TA829, 1:200, *red*, *arrow*) and nuclei (DAPI, *blue*) of cultured neonatal cardiomyocyte. The immunoreactive signal in the plasma membrane was remarkably reduced following transfection of AGS8siRNA1 or AGS8siRNA2 (*right panels*). The data are representative of four independent experiments with similar results. *C*, analysis of subcellular localization of AGS8 by immunoelectron microscopy. The fixed mouse heart section was subjected to immunoelectron microscopy as described under supplemental data. AGS8 signals were identified in the cellular junction (*left panel*, ×18,500) as well as mitochondria (*right panels*, ×11,100).

negative controls, respectively. The incorporated biotinylated dCTP was then detected with strepavidin-peroxidase conjugate and revealed in 0.5 mg/ml diaminobenzidine for 10 min. Nuclear brown staining was viewed under a light microscope.

Assessment of Mitochondrial Membrane Potential—Loss of mitochondrial membrane potential was assessed with a fluorescence microscope (Nikon TE2000U microscope, NIKON, Tokyo, Japan) after staining with MitoCapture (BioVision, Moutain View, CA), in which cells were stained with a cationic dye that fluoresced differently in healthy *versus* apoptotic cells. Cardiomyocytes were incubated MitoCapture for 15 min at 37 °C. After the dye was applied, images were captured by fluorescence microscopy within 30 min with microscope. A 488-nm filter and 543-nm filter were used for excitation, and the resultant red and green fluorescence were quantified with

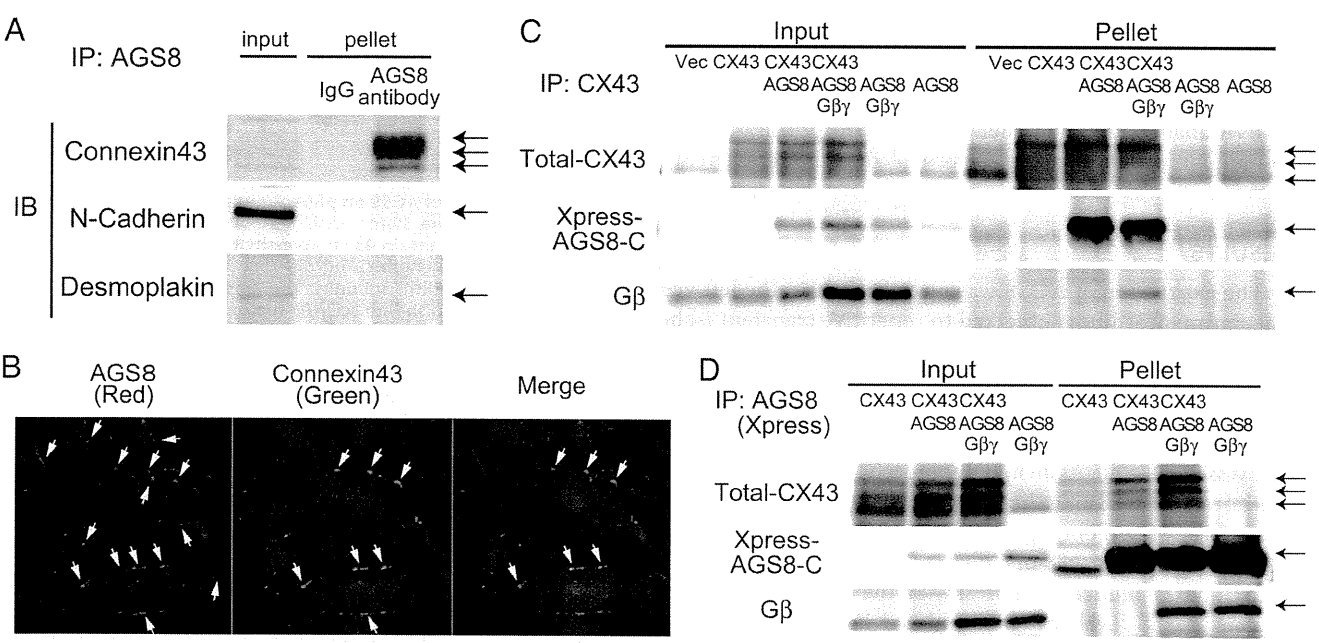

FIGURE 4. **Association of AGS8 with connexin 43.** *A*, determination of junctional proteins co-immunoprecipitated by anti-AGS8 antibody (TA829). Tissue preparation and immunoprecipitation were performed as described under supplemental data. Connexin 43 was co-immunoprecipitated by AGS8 antibody (TA829, 3.5 μg) from −1 mg of solubilized crude membrane of rat left ventricle in immunoprecipitation (IP) buffer (50 mM Tris, pH 7.4, 150 mM NaCl, 5 mM EDTA, 1% Igepal CA-630, a protease inhibitor tablet-Complete Mini (Roche Applied Science)). *B*, detection of co-localization of AGS8 with connexin 43. Cultured neonatal cardiomyocytes were fixed and stained for AGS8 (*left panel*, TA829 antibody, 1:200, *red*, *arrow*), connexin 43 (*middle panel*, mouse monoclonal connexin 43 antibody (MAB3068, CHEMICON), 1:100, *green*, *arrow*), and nuclei (DAPI, *blue*). Co-localization of connexin 43 with AGS8 (*yellow*, *arrow*) is shown in the *right panel* (*merge*). *C* and *D*, an interaction of C-terminal AGS8 (AGS8-C) with connexin 43 and/or Gβγ subunit. COS7 cells in a 100-mm dish were transfected with a combination of pcDNA3, pMH::connexin 43 (3 μg/dish), pcDNAHis::AGS8-C (6 μg/dish), pcDNA3::$G\beta_1$ (1.5 μg/dish), and/or pcDNA3::$G\gamma_2$ (1.5 μg/dish). The amount of DNA transfected was adjusted to 12 μg per dish with pcDNA3 vector. The preparation of cell lysate and immunoprecipitation was performed as described under supplemental data. AGS8-C was immunoprecipitated by 1.5–2 μg of CX43 antibody (*C*) or Xpress antibody (*D*) from 500–800 μg of cell lysate in IP buffer, and the pellet was subjected to immunoblot to detect protein as indicated in the figure. The transferred membrane was reprobed with antibodies as indicated in the figure. The data are representative of five independent experiments with similar results.

GFP-B (NIKON, Tokyo, Japan) and TRITC (NIKON, Tokyo, Japan) filters, respectively. The red emission of the dye is due to a potential-dependent aggregation in the mitochondria reflecting normal membrane potential. Green fluorescence reflects the monomeric form of MitoCapture, appearing in the cytosol after mitochondrial membrane depolarization (16).

Dye Uptake Study—Cells were incubated with 1 mM Lucifer Yellow (LY) (Molecular Probes) for 30 or 45 min in normal culture medium. Unincorporated LY was removed, and cells were rinsed with phosphate-buffered saline. The fluorescence of LY was immediately evaluated by fluorescence microscopy (B-3A filter, TE2000-E, NIKON, Tokyo, Japan). The signal intensity of fluorescence of LY was quantified in 10 randomly selected fields (10 × 20) using NIS-Elements 3.0 software (NIKON, Tokyo, Japan). The non-selective binding of LY was determined by fluorescence in the presence of a connexin hemichannel blocker, 50 μM Lanthanum (Sigma-Aldrich), which was added 30 min prior to LY.

Miscellaneous Procedures and Statistical Analysis—Immunoblotting and data analysis were performed as described previously (7, 8, 17). The luminescence images captured with an image analyzer (LAS-3000, FUJIFILM, Tokyo, Japan) were quantified using Image Gauge 3.4 (FUJIFILM, Tokyo, Japan). Data are presented as mean ± S.E. from independent experiments as described in the figure legends. Statistics were performed using two-way and/or one-way ANOVA by Tukey's multiple comparison post-hoc test otherwise indicated in the text. All statistical analyses were performed with Prism 4 (GraphPad Software).

Supplemental Data—Additional information on preparation of cardiomyocytes, cell culture, detection of apoptosis, AGS8 mRNA analysis, immunochemistry, protein preparation, and immunoprecipitation assay are provided in the supplemental data.

RESULTS

The expression of AGS8 was up-regulated in the left ventricular myocardium subjected to repetitive transient ischemia, suggesting that AGS8 might be involved in adaptation processes in an ischemic myocardium (8). Such events might include the initiation of cell death or acquisition of tolerance to ischemic injury in conjunction with the development of collateral vessels (18–20). As an initial approach to identify the physiological role of AGS8 in the heart, we investigated its involvement in the survival of cardiomyocytes following hypoxic stress.

Suppression of AGS8 in Cultured Cardiomyocytes Attenuates Hypoxia-induced Apoptosis—In the first series of experiments, AGS8 level was manipulated in cultured neonatal cardiomyocytes (NCM) before exposure to hypoxia, and their survival rate was monitored. Small interfering RNA (siRNAs) for AGS8 (AGS8siRNA) targeted two distinct regions in AGS8 (Fig. 1*A*). The effect of AGS8siRNA and control siRNA oligonucleotides on expression of AGS8 was determined in NCM (Fig. 1*B*). Both AGS8siRNAs, but not their controls, successfully suppressed the level of AGS8 of cardiomyocytes to ~30% of the level of cardiomyocytes treated with negative control siRNA.

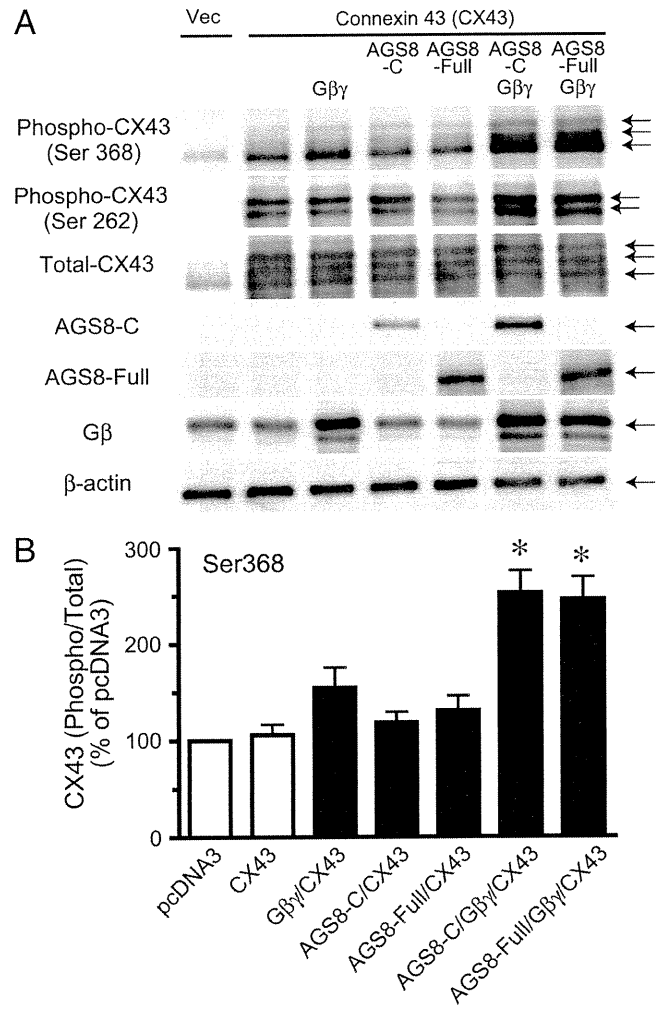

FIGURE 5. **Influence of AGS8 on phosphorylation of connexin 43 in COS7 cell.** COS7 cells in the 35-mm dish were transfected with a combination of pcDNA3, pMH::connexin 43 (1 μg/dish), pcDNAHis::AGS8-C (2 μg/dish), pcDNAHis::AGS8-full-length (2 μg/dish), pcDNA3::$G\beta_1$ (1 μg/dish), and/or pcDNA3::$G\gamma_2$ (1 μg/dish) subunits. The amount of DNA transfected was adjusted to 5 μg per dish with pcDNA3 vector. After 48 h of transfection, cells were solubilized into Laemmli buffer, and 10 μg of cell lysates were subjected to SDS-PAGE. *A*, phosphorylated CX43 was detected phospho-CX43 antibody for serine 368 or serine 262. The expression of AGS8-C or AGS8-full-length was detected by Xpress antibody (1:5000) or TB087101 (1:1000), respectively. The data are representative of four independent experiments with similar results. *B*, densitometric analysis of the immunoreactive signals shown in *A*. The level of phosphorylated connexin 43 (Ser-368) was normalized with total connexin 43 and expressed as percent of pcDNA3-transfected control. *Vec*, pcDNA3; *AGS8-C*, 372 amino acids of the C-terminal region of AGS8; *AGS8-F*, full-length of AGS8. *, $p < 0.05$ *versus* connexin 43 alone. $n = 7$ from four independent experiments.

48 h after transfection with the siRNAs, NCMs were exposed to 1% O_2 hypoxia or normoxia for 6 or 24 h to induce hypoxia-mediated cell death. Hypoxic stress markedly increased the number of apoptotic cardiomyocytes and this was completely blocked by knockdown of AGS8 (Fig. 2*A*). Suppression of AGS8 alone did not influence the number of TUNEL-positive cells cultured in normoxic conditions throughout the experimental period[5] and control siRNA oligonucleotides were without effect.

[5] T. Honda, and M. Sato, unpublished observations.

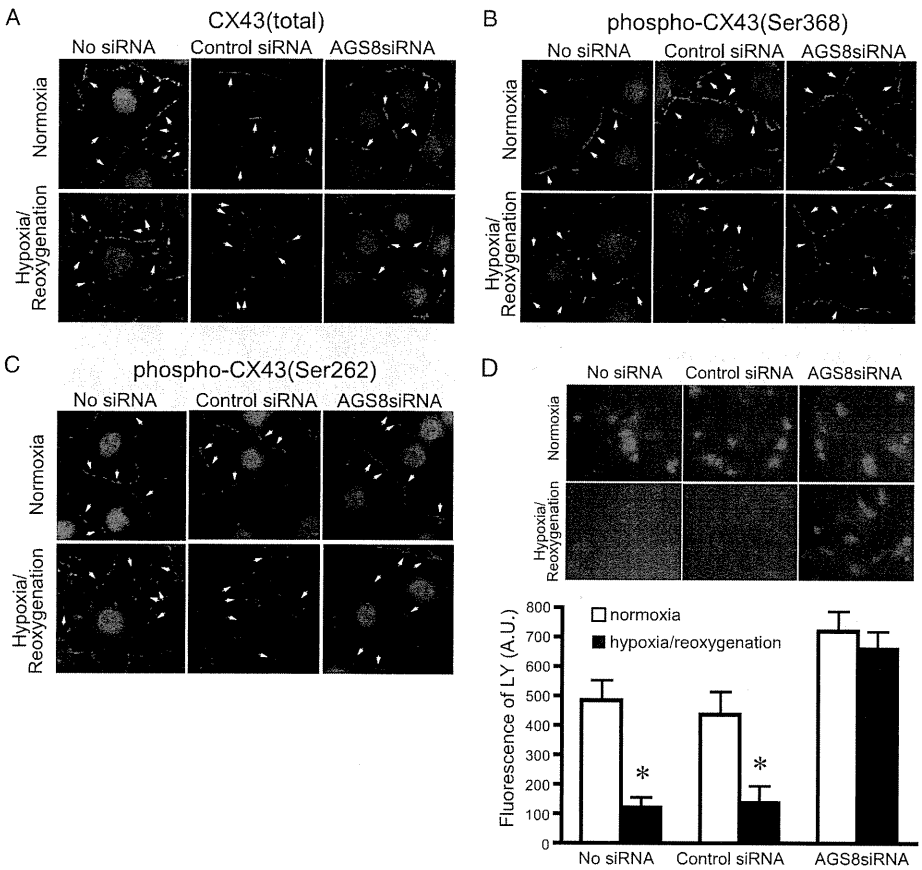

FIGURE 6. **Influence of AGS8 on hypoxia-induced internalization and the change of permeability of in cardiomyocytes.** *A–C*, an effect of AGS8siRNA on internalization of CX 43. Cardiomyocytes were exposed 3 times to 30 min of hypoxia intermittant with 30 min of reoxygenation 48 h after (without or with) transfection of universal negative siRNA control (Control siRNA) or AGS8siRNA2 (AGS8siRNA). After the third hypoxic period, cells were immediately fixed and subjected to immunofluorescence stain for total CX43 (*A*), phospho-CX43 (Ser-368) (*B*), or phospho-CX43 (Ser-262) (*C*) as described under "Experimental Procedures." For the detection of phospho-CX43, 8 μM MG132 was added to the culture prior to sequential hypoxia. The figures demonstrated the triple stain of CX43 (*red, arrow*), N-cadherin (*green*), and nuclei (DAPI, *blue*). The data are representative of 4–6 independent experiments with similar results. *D*, uptake of fluorescence dye, LY, bu the cardiomyocytes. The fluorescence of LY was evaluated by microscopy as described under "Experimental Procedures." *Upper panel*, representative pictures of cardiomyocytes incorporating LY. *Lower panel*, fluorescence of LY was quantified by the intensity of fluorescence of 10 randomly selected fields (10 × 20). *, $p < 0.05$ *versus* cells at normoxia. $n = 4$ from four independent experiments.

Suppression of AGS8 Reduced Apoptosis Induced by Hypoxia/Reoxygenation—Reoxygenation following hypoxic periods accelerates apoptosis of cardiomyocytes (21). The influence of AGS8 on apoptosis of cardiomyocytes induced by hypoxia/reoxygenation was also examined by sequential exposure of cardiomyocytes to hypoxia (1%, O_2) for 6 h, followed by normoxia for 18 h in siRNA-transfected NCM.

Interestingly, both AGS8siRNAs blocked apoptosis of cardiomyocytes following hypoxia/reoxygenation. In this protocol, the hypoxia/reoxygenation induced apoptosis of cardiomyocytes in control groups (non-transfected control, 437 ± 29.7% increase *versus* normoxia group; Fig. 2*B*), and the number of TUNEL-positive cells was increased as compared with 6 h of straight hypoxia alone (non-transfected control, 289.8 ± 14.0% *versus* normoxia group; Fig. 2*A*).

The effect of AGS8siRNA on apoptosis was verified in another approach by detecting the change of mitochondrial membrane potential. As observed in TUNEL, AGS8siRNA blocked the loss of membrane potential of the mitochondria (Fig. 2*C*) (22, 23).

Overexpression of AGS8 Increased Apoptosis following Hypoxia/Reoxygenation—The striking effects of AGS8siRNA on hypoxia-induced apoptosis suggested that AGS8 was required for hypoxia-mediated death of cardiomyocytes and behaved as a proapoptotic factor under hypoxic stress. However, these effects were observed by suppression of AGS8. On the other hand, AGS8 was up-regulated in the myocardium subjected to repetitive ischemia in which AGS8 was originally identified (8). Accordingly, we introduced pDNA3::AGS8 to cardiomyocytes utilizing a viral envelope system and evaluated its effect on apoptosis (Fig. 2*D*). The transfection efficiency of this procedure was ~50–60%, as estimated by fluorescence of the pEGFP vector. The number of TUNEL-positive cells increased following exposure to hypoxia (6 h)/reoxygenation (18 h) in both of cardiomyocytes transfected with pcDNA3 alone or pcDNA3::AGS8. However, the magnitude of increase in the number of TUNEL-positive cells was significantly greater in AGS8-transfected cells. Notably, the expression level of AGS8 alone did not influence the number of apoptotic cells cultured in normoxia as observed in the series of experiments with siRNAs, suggesting that the a specific function of AGS8 was revealed in response to hypoxic stress.

AGS8 was Enriched in the Plasma Membrane of Cardiomyocytes—Hypoxia-mediated cell death is involved in multiple signaling events occurring in plasma membranes and organelles in the cytosol as well as the nucleus. The ability of accessory proteins for G-proteins to influence cellular events is sometimes critically regulated by their subcellular localization or distribution (4). We next determined the localization of AGS8 in cardiomyocytes manipulating cellular events under hypoxic conditions. To address this issue, we developed an antibody against AGS8. Affinity-purified AGS8 antibody (TA829) recognized AGS8 expressed in COS7 cells by immunoblot (Fig. 1*C*). In the immunofluorescence stain, TA829 detected immunoreactive signals of AGS8 expressed in COS7 cells (Fig. 1*D*).

AGS8 antibody (TA829) recognized an immunoreactive signal in the plasma membrane of the left ventricle as well as cul-

tured cardiomyocytes (Fig. 3, *A* and *B*). Interestingly, the signals were enriched at the cell-cell interface and were attenuated in the cultured NCM following transfection of siRNAs for AGS8. The transfection of universal negative siRNA control (Stealth RNAi Negative Control) did not influence on the immunoreactive signals detected by AGS8 antibody (TA829) (supplemental Fig. S1*A*).

The localization of AGS8 in the microdomain of cells was further investigated by immunoelectronmicroscopy. AGS8 was observed in the junctional regions of plasma membrane (Fig. 3*C*, *arrowhead*) as well as the surface of mitochondria (Fig. 3*C*, *arrow*) where multiple events related to apoptosis are processed. No immunoreactive signals were detected in the absence of AGS8 antibody (supplemental Fig. S1*B*). These observations suggest that AGS8 assembles a complex with proteins in cellular junctions (24).

AGS8 Formed Protein Complexes with CX43—The possible formation of AGS8 complexes with junctional proteins was addressed by immunoprecipitation assays using the AGS8 antibody (TA829), which successfully immunoprecipitated expressed AGS8 from cell lysates (Fig. 1*E*). Interestingly, TA829 co-immunoprecipitated channel protein CX43 from rat ventricular lysate, but not other proteins typically comprising the adherence junction or desmosome, such as N-cadherin and desmoplakin, respectively (Fig. 4*A*) (24). The immunoblot of CX43 indicated enrichment of a slower migrating species upon immunoprecipitation that likely represents phosphorylated CX43 (Fig. 4*A*) (25, 26). Immunofluorescence studies also indicated co-localization of AGS8 and CX43 in cultured NCM (Fig. 4*B*). AGS8 signals were recognized in a broader area as compared with CX43, suggesting that a population of AGS8 exists apart from CX43.

Subsequent studies with transfected COS7 cells indicated that the C-terminal region of AGS8 (AGS8-C), which bound to $G\beta\gamma$, was co-immunoprecipitated by CX43 antibody (Fig. 4*C*) (8, 14). $G\beta\gamma$ also co-immunoprecipitated in the pellet with AGS8 and CX43. Conversely, CX43 was co-immunoprecipitated by Xpress antibody for AGS8-C (Fig. 4*D*). $G\beta\gamma$ was again co-immunoprecipitated with AGS8 and CX43 suggesting that $G\beta\gamma$ is involved in the assembly of the AGS8-CX43 complex.

CX43 is a transmembrane protein forming channels that pass multiple small molecules including adenosine 5′-triphosphate, adenosine, cAMP, inositol-1,4,5-trisphosphate (27–29). CX43 localized at gap junctions, plasma membranes as well as mitochondria of cardiomyocytes where AGS8 was also detected (Fig. 3) (30–32). Previous observations clearly indicated the involvement of CX43 in the ischemia/hypoxia-induced apoptosis of cardiomyocytes via alteration of cell permeability to small molecules (26, 33–36). The phosphorylation status and subcellular localization of CX43 are suggested to be critical for the apoptotic process of cells under hypoxic stress (26, 33, 34, 36).

AGS8 may regulate hypoxia-induced apoptosis via CX43 as an unexpected target of G-protein signaling. Therefore, the effects of AGS8 on the regulation of CX43 were addressed by determining the impact of altered AGS8 expression in cardiomyocytes on CX43 phosphorylation, CX43 subcellular distribution and CX43 permeability before and during hypoxic stress.

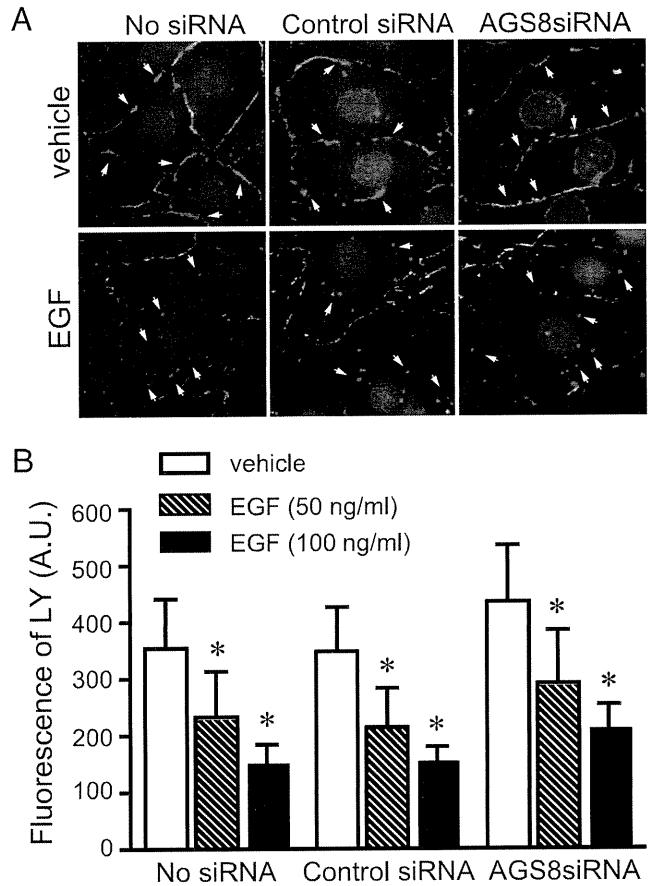

FIGURE 7. **Influence of AGS8 on EGF-induced internalization of CX43 and change of permeability.** *A*, an effect of AGS8siRNA on internalization of CX43. Cardiomyocytes were stimulated by 100 ng/ml EGF for 30 min 48 h after (without or with) transfection of universal negative siRNA control (Control siRNA) or AGS8siRNA2 (AGS8siRNA). Cells were immediately fixed and subjected to immunofluorescence stain for total CX43 as described under "Experimental Procedures." The figures demonstrated the triple stain of CX43 (*red*, *arrow*), N-cadherin (*green*), and nuclei (DAPI, *blue*). The data are representative of four independent experiments with similar results. *B*, uptake of fluorescence dye, LY, by the cardiomyocytes. The fluorescence of LY was evaluated by microscopy as described under "Experimental Procedures." The fluorescence of LY was quantified by the intensity of fluorescence of 10 randomly selected fields (10 × 20). *, $p < 0.05$ in one-way ANOVA. No statistical significance was observed among groups in two-way ANOVA. $n = 4$ from four independent experiments.

AGS8 Stimulated Phosphorylation of CX43 in a Gβγ-dependent Manner—The effect of AGS8 on CX43 phosphorylation and the involvement of $G\beta\gamma$ were determined in transiently transfected COS7 cells (Fig. 5, *A* and *B*). The expression of $G\beta\gamma$ or AGS8 alone did not influence the phosphorylation level of CX43. However, CX43 phosphorylation was significantly increased when cells were simultaneously transfected with AGS8 and $G\beta\gamma$. AGS8-$G\beta\gamma$ stimulated phosphorylation of serine 368 as well as serine 262 on CX43, indicating AGS8 and $G\beta\gamma$ regulated multiple phosphorylation sites of CX43. Furthermore, AGS8-C also stimulated phosphorylation of CX43 in the presence of $G\beta\gamma$, suggesting the functional importance of the C-terminal region of AGS8 and $G\beta\gamma$ input for CX43 phosphorylation. Because the level of phosphorylated CX43 was higher

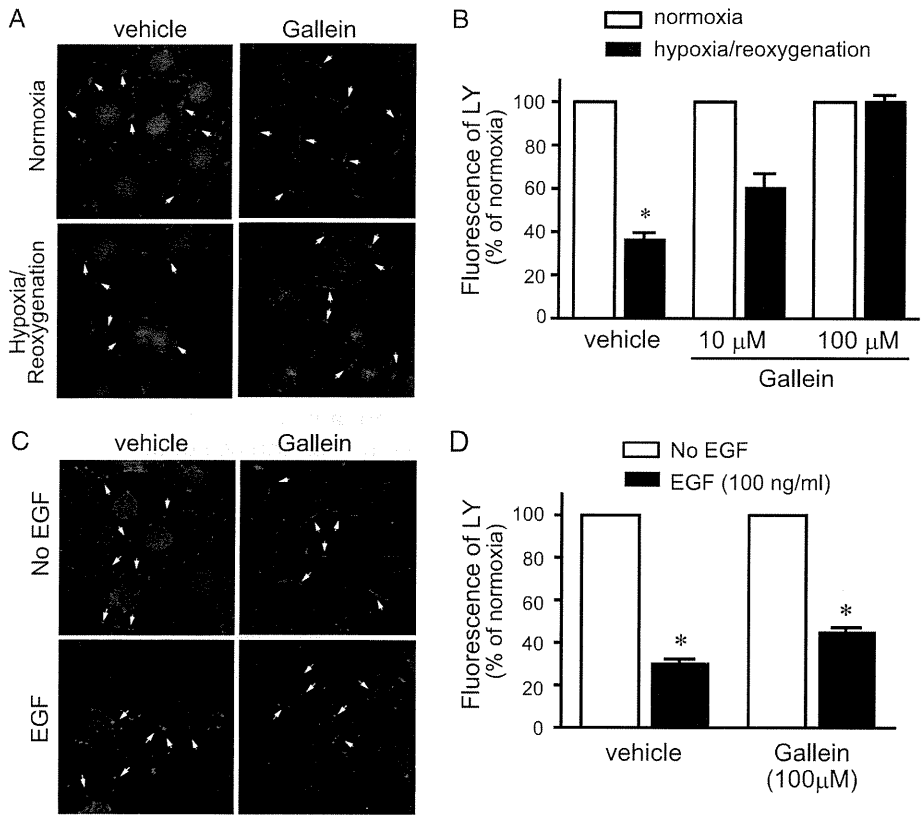

FIGURE 8. **Effect of Gallein on internalization and change of permeability of CX43 induced by hypoxia or EGF.** *A*, an effect of Gallein on internalization of CX 43. Cardiomyocytes were exposed 3 times to 30 min of hypoxia intermittant with 30 min of reoxygenation. After the third hypoxic period, cells were immediately fixed and subjected to immunofluorescence stain for total CX43 as described under "Experimental Procedures." The figures demonstrated the double stain of CX43 (*red, arrow*) and nuclei (DAPI, *blue*). The data are representative of four independent experiments with similar results. *B*, uptake of fluorescence dye, LY, by the cardiomyocytes. The fluorescence of LY was evaluated by microscopy as described under "Experimental Procedures." The fluorescence of LY was quantified by the intensity of fluorescence of 10 randomly selected fields (10 × 20). *, $p < 0.05$ in Kruskal-Wallis test followed by Dunn's multiple comparison post-hoc test. $n = 4$ from four independent experiments. *C*, an effect of Gallein on internalization of CX43. Cardiomyocytes were stimulated by 100 ng/ml EGF for 30 min, then cells were immediately fixed and subjected to immunofluorescence stain for total CX43. The figures demonstrated the double stain of CX43 (*red, arrow*) and nuclei (DAPI, *blue*). The data are representative of four independent experiments with similar results. *D*, uptake of fluorescence dye, LY, by cardiomyocytes. The fluorescence of LY was evaluated by microscopy as described under "Experimental Procedures." The fluorescence of LY was quantified by the intensity of fluorescence of 10 randomly selected fields (10 × 20). *, $p < 0.05$ *versus* control without EGF stimulation in Kruskal-Wallis test followed by Dunn's multiple comparison post-hoc test. $n = 4$ from four independent experiments.

when cells were co-transfected with AGS8 and Gβγ compared with cells transfected with Gβγ alone, these data suggest that AGS8 served as a scaffold to facilitate phosphorylation of CX43, rather than simply releasing free Gβγ from Gα to activate Gβγ signaling.

The Requirement of AGS8 for Hypoxia-mediated Internalization of CX43—The phosphorylation of CX43 is associated with its internalization as well as turnover of the protein (30, 37, 38). An impact of AGS8siRNA on internalization of CX43 was determined in NCM following hypoxic stress. The large part of CX43 was observed in the cell surface, which was detected by N-cadherin (Fig. 6*A*). Exposure of cardiomyocytes to repetitive hypoxia induced internalization of CX43 in NCM with non-transfection as well as control siRNA (Fig. 6*A*). However, AGS8siRNA2 remarkably blocked the internalization of CX43 induced by repetitive hypoxia.

The hypoxia-induced internalization of CX43 was also associated with increased CX43 phosphorylation (30, 39). The immunofluoresence signals of phosphorylated CX43 were greatly enhanced in the presence of the proteasome inhibitor MG132, suggesting rapid degradation of phosphorylated CX43 as previously reported (30, 37). The majority of phosphorylated CX43 detected by serine 368 or serine 262 antibodies were observed in the cytoplasm following repetitive hypoxia in non-transfected NCMs as well as in the control siRNA group (Fig. 6, *B* and *C*). However, phosphorylated CX43 remained at the cell surface following knockdown of AGS8, suggesting a pivotal role of AGS8 in the internalization of CX43. A similar effect of AGS8 knockdown was also observed AGS8siRNA1 (supplemental Fig. S2*A*).

AGS8 Preserved Permeability of Small Molecule Flow Through CX43 Following Repetitive Hypoxia—The loss of hemichannel CX43 from the cell surface decreases influx and efflux of small molecules through CX43. AGS8-mediated regulation of CX43 may influence the permeability of small molecules involved in the fate of NCM under hypoxia. To address this issue, we examined the flux of dye through CX43 before and during hypoxic stress. Lucifer Yellow (LY) in the culture medium was incorporated into NCMs in a time-dependent manner.[6] Repetitive hypoxia decreased the accumulation of LY to 27.4 ± 4.9% ($p < 0.05$) in the non-transfected NCM or 34.1 ± 10.6% ($p < 0.05$) in control siRNA-transfected NCM compared with normoxia groups, respectively (Fig. 6*D*). However, interestingly, the permeability of CX43 was maintained in the NCM transfected with AGS8siRNA (93.1 ± 6.9% *versus* normoxia, no statistical significance). This observation was consistent with immunofluorescence studies in which CX43 remained at the cell surface following repetitive hypoxia by knockdown of AGS8 (Fig. 6, *A–C*).

AGS8 was not Involved in Receptor-mediated Internalization of CX43—We next investigated if AGS8 regulated CX43 as a part of adaptive program of NCM in response to "hypoxic stress" or AGS8 is merely involved in the "general pathway" of

[6] Q. Jiao, and M. Sato, unpublished observations.

internalization of CX43. To address this issue, the effect of AGS8siRNA2 on receptor-mediated internalization of CX43 was examined. EGF stimulated phosphorylation of CX43 via the mitogen-activated protein kinase pathway that led to internalization of CX43 (37). EGF induced internalization of CX43 in non-transfected NCMs as well as control siRNA-transfected NCMs (Fig. 7*A*). In contrast to the effect of AGS8 knockdown on hypoxia-mediated internalization of CX43, AGS8siRNA did not alter EGF-mediated internalization of CX43. A similar result was observed with AGS8siRNA1 (supplemental Fig. S2*B*).

The accumulation of LY inside the cells is consistent with the influence of EGF on CX43 internalization. EGF decreased the permeability of CX43 in a dose-dependent manner, reflecting loss of CX43 at the cell surface (Fig. 7*B*). The permeability of CX43 was decreased in all of the groups to a similar extent. These observations were in contrast with the impact of AGS8siRNA in repetitive hypoxia, suggesting the AGS8-mediated signal was activated under hypoxic stress.

The Involvement of the Gβγ Signal in the Internalization of CX43—AGS8 was identified as a receptor-independent Gβγ signal regulator induced in the ischemic myocardium. AGS8 formed a scaffold with CX43/Gβγ in cells (Figs. 3 and 4), and stimulated phosphorylation of CX43 in a Gβγ-dependent manner (Fig. 5), suggesting that activation of the Gβγ signal is involved in the regulation of CX43. Thus, we examined the change of internalization and permeability of CX43 following treatment with the Gβγ signal inhibitor, Gallein, which occupied a "common" interaction surface of Gβγ and inhibited its interaction with Gβγ-regulated proteins (40).

Interestingly, Gallein blocked internalization of CX43 (Fig. 8*A*) and maintained LY uptake under repetitive hypoxia in a dose-dependent manner (Fig. 8*B*). Thus, Gallein mimicked the effect of AGS8siRNA in the regulation of CX43 upon hypoxic stress. Next, the effect of Gallein on EGF-mediated internalization of CX43 was further investigated. As observed with AGS8siRNA, Gallein did not block EGF-mediated internalization of CX43 nor block the decrease of LY uptake following EGF treatment, suggesting AGS8siRNA and Gβγ signal inhibitor had comparable effects on the regulation of CX43 in NCM (Fig. 8, *C* and *D*).

DISCUSSION

Here, we demonstrated the requirement of AGS8 for hypoxia-mediated apoptosis of cardiomyocytes. Interestingly, knockdown of an accessory protein for heterotrimeric G-proteins had a remarkable effect on survival of cardiomyocytes under hypoxic stress. The observations suggested the pivotal role of AGS8 in hypoxia-mediated cell death and the potential as a therapeutic target in selected pathologies. AGS8 altered the sensitivity of cardiomyocytes to hypoxic stress rather than constitutively activating the apoptotic pathway, since proapoptotic effects of AGS8 were not observed in cells cultured under normoxia. Subsequent experiments indicated that this reorganization was associated with internalization of CX43 as well as an associated reduction in permeability of small molecules (Fig. 9). We demonstrated that the ischemia-inducible G protein regulator, AGS8 altered survival of cardiomyocyte under hypoxia,

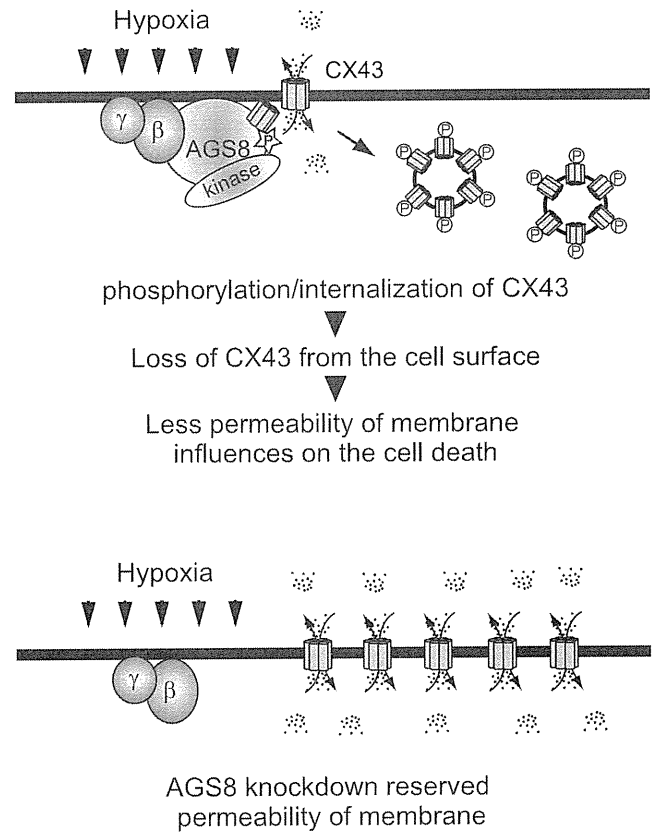

FIGURE 9. **Schematic diagram indicating roles of AGS8 in regulation of connexin 43 in cardiomyocytes.** *Upper panel*, AGS8 elicits phosphorylation of CX43 by serving as scaffold including CX43, Gβγ, and kinases. Phosphorylated CX43 leads to internalization of CX43 and decrease of channels in the plasma membrane. The decreased permeability of small molecule flow through CX43 influences apoptotic cell death under hypoxic stress. *Lower panel*, CX43 are not down-regulated following AGS8 knockdown by siRNA. The permeability of CX43 is maintained under hypoxic stress that may contribute to survival of cells.

which was associated with Gβγ-mediated regulation of CX43. Such activation of inherent programs involving a G protein regulator are particularly interesting for understanding the mechanism of cardiovascular disease.

Our data indicated that activation of Gβγ signaling was required for the hypoxia-induced CX43 internalization. The significant correlation of AGS8 with Gβγ suggested that AGS8 activated Gβγ pathway in response to hypoxic stress. The Gβγ regulator AGS8 formed a scaffold with CX43/Gβγ in cells and stimulated phosphorylation of CX43 with Gβγ (Figs. 3–5). Both AGSsiRNA and Gβγ signal inhibitor Gallein blocked the hypoxia-induced internalization of CX43 but not receptor-mediated internalization. AGS8 promoted Gβγ signal in cells as we demonstrated (8). These data suggest that AGS8 is involved in the activation of Gβγ signaling as a part of an adaptive program of NCM in the face of hypoxia that leads CX43 to internalization.

Ischemic injury of the myocardium is caused by the activation of multiple cascades initiating intracellular ionic and chemical changes that lead to cell death (21, 23). The channel protein CX43 is clearly involved in the apoptotic process by regulating the permeability of small molecules including aden-

osine 5′-triphosphate, adenosine diphosphate, adenosine, cAMP, inositol-1,4,5-trisphosphate, glutamate, and glutathione (26–29, 33). AGS8 reorganized cellular environments to be sensitive to hypoxic stress, at least in part, by controlling permeability of such molecules flowed through CX43. Functions of connexins are influenced by their phosphorylation and subcellular localization as well as protein turnover (36–38). Each step of regulation affects the fate of cells depending on the type of stress experienced by the cells (27, 35, 39, 41). In response to ischemia/hypoxia, AGS8 apparently coordinates the generation of a scaffold that includes CX43, $G\beta\gamma$ and possibly kinases that initiates CX43 phosphorylation leading to closure, internalization, and degradation of CX43 (27, 30, 36–38). Such a regulatory mechanism may play a critical role in the survival of cardiomyocytes under particular conditions. In contrast to our observations demonstrating the association of hypoxia-induced apoptosis with dynamic regulation of CX43, the reduction of CX43 itself did not show a significant effect on myocardial infarction in the heterozygous deletion mice ($CX43^{+/-}$) (35, 42), suggesting different adaptation mechanisms in the two challenges.

The adaptation program of cardiomyocytes to ischemia/hypoxia included the unexpected regulation of G-proteins and CX43 by AGS8. It would be important to validate the role of AGS8 and its association with CX43 in multiple systems including adult ventricular cardiomyocytes as well as a whole body model under various types of stress. Although the additional proteins involved in the phosphorylation as well as internalization of CX43 has yet to be determined, an investigation into the disruption of the AGS8 cascade may shed light on an approach for protection against cardiac ischemic injury.

Acknowledgments—We thank Dr. Akira Akatsuka (Teaching and Research Support Center, Tokai University School of Medicine, Isehara, Kanagawa, Japan) for technical support for electronmicroscopy.

REFERENCES

1. Birnbaumer, L. (2007) *Biochim. Biophys. Acta* **1768,** 772–793
2. Smrcka, A. V. (2008) *Cell Mol. Life Sci.* **65,** 2191–2214
3. Oldham, W. M., and Hamm, H. E. (2006) *Q. Rev. Biophys.* **39,** 117–166
4. Sato, M., Blumer, J. B., Simon, V., and Lanier, S. M. (2006) *Annu. Rev. Pharmacol. Toxicol.* **46,** 151–187
5. Cismowski, M. J. (2006) *Semin Cell Dev. Biol.* **17,** 334–344
6. Blumer, J. B., Smrcka, A. V., and Lanier, S. M. (2007) *Pharmacol. Ther.* **113,** 488–506
7. Sato, M., Gettys, T. W., and Lanier, S. M. (2004) *J. Biol. Chem.* **279,** 13375–13382
8. Sato, M., Cismowski, M. J., Toyota, E., Smrcka, A. V., Lucchesi, P. A., Chilian, W. M., and Lanier, S. M. (2006) *Proc. Natl. Acad. Sci. U.S.A.* **103,** 797–802
9. Blumer, J. B., Lord, K., Saunders, T. L., Pacchioni, A., Black, C., Lazartigues, E., Varner, K. J., Gettys, T. W., and Lanier, S. M. (2008) *Endocrinology* **149,** 3842–3849
10. Sato, M., and Ishikawa, Y. (2009) *Pathophysiology,* 10.1016/j.pathophys.2009.03.011
11. Hendriks-Balk, M. C., Peters, S. L., Michel, M. C., and Alewijnse, A. E. (2008) *Eur. J. Pharmacol.* **585,** 278–291
12. Heximer, S. P., Srinivasa, S. P., Bernstein, L. S., Bernard, J. L., Linder, M. E., Hepler, J. R., and Blumer, K. J. (1999) *J. Biol. Chem.* **274,** 34253–34259
13. Rogers, J. H., Tamirisa, P., Kovacs, A., Weinheimer, C., Courtois, M., Blumer, K. J., Kelly, D. P., and Muslin, A. J. (1999) *J. Clin. Invest.* **104,** 567–576
14. Yuan, C., Sato, M., Lanier, S. M., and Smrcka, A. V. (2007) *J. Biol. Chem.* **282,** 19938–19947
15. Yogo, K., Ogawa, T., Akiyama, M., Ishida, N., and Takeya, T. (2002) *FEBS Lett.* **531,** 132–136
16. Li, J., Niu, X. L., and Madamanchi, N. R. (2008) *J. Biol. Chem.* **283,** 34260–34272
17. Sato, M., Ribas, C., Hildebrandt, J. D., and Lanier, S. M. (1996) *J. Biol. Chem.* **271,** 30052–30060
18. Toyota, E., Warltier, D. C., Brock, T., Ritman, E., Kolz, C., O'Malley, P., Rocic, P., Focardi, M., and Chilian, W. M. (2005) *Circulation* **112,** 2108–2113
19. Hausenloy, D. J., and Yellon, D. M. (2007) *Pharmacol. Ther.* **116,** 173–191
20. Webster, K. A. (2007) *Trends Pharmacol. Sci.* **28,** 492–499
21. Yellon, D. M., and Hausenloy, D. J. (2007) *N. Engl. J. Med.* **357,** 1121–1135
22. Cook, S. A., Sugden, P. H., and Clerk, A. (1999) *Circ. Res.* **85,** 940–949
23. Bishopric, N. H., Andreka, P., Slepak, T., and Webster, K. A. (2001) *Curr. Opin. Pharmacol.* **1,** 141–150
24. Saffitz, J. E. (2005) *Ann. N.Y. Acad. Sci.* **1047,** 336–344
25. Lampe, P. D., Cooper, C. D., King, T. J., and Burt, J. M. (2006) *J. Cell Sci.* **119,** 3435–3442
26. Solan, J. L., Marquez-Rosado, L., Sorgen, P. L., Thornton, P. J., Gafken, P. R., and Lampe, P. D. (2007) *J. Cell Biol.* **179,** 1301–1309
27. Bao, X., Lee, S. C., Reuss, L., and Altenberg, G. A. (2007) *Proc. Natl. Acad. Sci. U.S.A.* **104,** 4919–4924
28. Rodríguez-Sinovas, A., Cabestrero, A., López, D., Torre, I., Morente, M., Abellán, A., Miró, E., Ruiz-Meana, M., and García-Dorado, D. (2007) *Prog. Biophys. Mol. Biol.* **94,** 219–232
29. Harris, A. L. (2007) *Prog. Biophys. Mol. Biol.* **94,** 120–143
30. Laird, D. W. (2005) *Biochim. Biophys. Acta* **1711,** 172–182
31. Ruiz-Meana, M., Rodríguez-Sinovas, A., Cabestrero, A., Boengler, K., Heusch, G., and Garcia-Dorado, D. (2008) *Cardiovasc. Res.* **77,** 325–333
32. Rodriguez-Sinovas, A., Boengler, K., Cabestrero, A., Gres, P., Morente, M., Ruiz-Meana, M., Konietzka, I., Miró, E., Totzeck, A., Heusch, G., Schulz, R., and Garcia-Dorado, D. (2006) *Circ. Res.* **99,** 93–101
33. Shintani-Ishida, K., Uemura, K., and Yoshida, K. (2007) *Am. J. Physiol. Heart Circ. Physiol.* **293,** H1714–H1720
34. Schulz, R., Gres, P., Skyschally, A., Duschin, A., Belosjorow, S., Konietzka, I., and Heusch, G. (2003) *Faseb J.* **17,** 1355–1357
35. Heinzel, F. R., Luo, Y., Li, X., Boengler, K., Buechert, A., García-Dorado, D., Di Lisa, F., Schulz, R., and Heusch, G. (2005) *Circ. Res.* **97,** 583–586
36. Ek-Vitorin, J. F., King, T. J., Heyman, N. S., Lampe, P. D., and Burt, J. M. (2006) *Circ. Res.* **98,** 1498–1505
37. Leithe, E., and Rivedal, E. (2004) *J. Cell Sci.* **117,** 1211–1220
38. Fernandes, R., Girão, H., and Pereira, P. (2004) *J. Biol. Chem.* **279,** 27219–27224
39. Turner, M. S., Haywood, G. A., Andreka, P., You, L., Martin, P. E., Evans, W. H., Webster, K. A., and Bishopric, N. H. (2004) *Circ. Res.* **95,** 726–733
40. Lehmann, D. M., Seneviratne, A. M., and Smrcka, A. V. (2008) *Mol. Pharmacol.* **73,** 410–418
41. Retamal, M. A., Schalper, K. A., Shoji, K. F., Bennett, M. V., and Sáez, J. C. (2007) *Proc. Natl. Acad. Sci. U.S.A.* **104,** 8322–8327
42. Schwanke, U., Konietzka, I., Duschin, A., Li, X., Schulz, R., and Heusch, G. (2002) *Am. J. Physiol. Heart Circ. Physiol.* **283,** H1740–H1742

Caveolin gene transfer improves glucose metabolism in diabetic mice

Koji Otsu, Yoshiyuki Toya, Jin Oshikawa, Reiko Kurotani, Takuya Yazawa, Motohiko Sato, Utako Yokoyama, Satoshi Umemura, Susumu Minamisawa, Satoshi Okumura and Yoshihiro Ishikawa

Am J Physiol Cell Physiol 298:C450-C456, 2010. First published 18 November 2009; doi:10.1152/ajpcell.00077.2009

Am J Physiol Cell Physiol 298: C450–C456, 2010.
First published November 18, 2009; doi:10.1152/ajpcell.00077.2009.

Caveolin gene transfer improves glucose metabolism in diabetic mice

Koji Otsu,[1] Yoshiyuki Toya,[2] Jin Oshikawa,[2] Reiko Kurotani,[1] Takuya Yazawa,[3] Motohiko Sato,[1] Utako Yokoyama,[1] Satoshi Umemura,[2] Susumu Minamisawa,[1,4] Satoshi Okumura,[1] and Yoshihiro Ishikawa[1,5]

[1]*Cardiovascular Research Institute,* [2]*Department of Cardiorenal Medicine, and* [3]*Department of Pathobiology, Yokohama City University Graduate School of Medicine, Yokohama, Japan;* [4]*Consolidated Research Institute for Advanced Science and Medical Care, Waseda University, Tokyo, Japan; and* [5]*Cardiovascular Research Institute, Departments of Cell Biology and Molecular Medicine and Medicine (Cardiology), New Jersey Medical School, Newark, New Jersey*

Submitted 9 March 2009; accepted in final form 4 November 2009

Otsu K, Toya Y, Oshikawa J, Kurotani R, Yazawa T, Sato M, Yokoyama U, Umemura S, Minamisawa S, Okumura S, Ishikawa Y. Caveolin gene transfer improves glucose metabolism in diabetic mice. *Am J Physiol Cell Physiol* 298: C450–C456, 2010. First published November 18, 2009; doi:10.1152/ajpcell.00077.2009.— Caveolin, a member of the membrane-anchoring protein family, accumulates various growth receptors in caveolae and inhibits their function. Upregulation of caveolin attenuates cellular proliferation and growth. However, the role of caveolin in regulating insulin signals remains controversial. Here, we demonstrate that caveolin potently enhances insulin receptor (IR) signaling when overexpressed in the liver in vivo. Adenovirus-mediated gene transfer was used to overexpress caveolin specifically in the liver of diabetic obese mice, which were generated with a high-fat diet. Expression of molecules involved in IR signaling, such as IR or Akt, remained unchanged after gene transfer. However, hepatic glycogen synthesis was markedly increased with a decrease in phosphoenolpyruvate carboxykinase protein expression. Insulin sensitivity was increased after caveolin gene transfer as determined by decreased blood glucose levels in response to insulin injection and fasting blood glucose levels. Glucose tolerant test performance was also improved. Similar improvements were obtained in *KKA*^{y} genetically diabetic mice. Adenovirus-mediated overexpression of caveolin-3 in hepatic cells also enhanced IR signaling, as shown by increased phosphorylation of IR in response to insulin stimulation and higher glycogen synthesis at baseline. These effects were attributed mostly to increased insulin receptor activity and caveolin-mediated, direct inhibition of protein tyrosine phosphatase 1B, which was increased in obese mouse livers. In conclusion, our results suggest that caveolin is an important regulator of glucose metabolism that can enhance insulin signals.

insulin receptor; diabetes mellitus

CAVEOLIN (CAV) IS COMPOSED of three subtypes (Cav1, Cav2, and Cav3), and it is a major protein component of caveolae, which are flask-shaped, cell membrane invaginations that are abundantly expressed in adipocytes, myocytes, and endothelial cells (5). Caveolae accumulate multiple receptors and kinases that are involved in cell growth and proliferation (11, 19). The net effect of these interactions is the suppression of cellular growth and proliferation signals (5). Accordingly, it is widely believed that Cav is a potent growth suppressor.

Despite numerous studies demonstrating an important role for Cav in regulating various growth signals, the role of Cav in regulating insulin receptor (IR) signals has remained rather controversial. Some studies have shown a positive association of Cav with IR signals (3, 22) while others have refuted these findings (10). Nevertheless, it has been proposed that Cav may not inhibit insulin signals, but may be required or even activate this signaling pathway (28). Mice with a disrupted Cav1 gene, which is most abundantly expressed in adipocytes, showed decreased IR protein expression and developed insulin resistance in fat tissues (7). Similarly, mice with disrupted Cav3, which is abundantly expressed in the muscles (9), developed insulin resistance in the skeletal muscles (22). Furthermore, a previous study used purified proteins to demonstrate that a small peptide derived from Cav stimulated IR kinase activity in vitro; interestingly, this stimulation was more potent with a peptide derived from Cav3 than Cav1 (30). These findings have suggested that Cav plays an important role in maintaining physiological insulin signals in the major target organs of insulin action, i.e., the liver and fat tissues.

In the present study, we have addressed the role of Cav in the liver. The liver is a major insulin target that expresses only a small amount of endogenous Cav, suggesting that the liver, unlike fat tissues and skeletal muscles, does not require high Cav levels, at least, under normal conditions. We have examined the effect of Cav3 gene transfer to the livers of diabetic obese mice fed a high-fat diet or *KKA*^{y} mice, a widely used Type 2 diabetic model (17). We demonstrated that Cav enhances IR signaling in vivo and in vitro. Insulin sensitivity and thus glucose metabolism were markedly improved by Cav3 gene transfer in diabetic mice, as exemplified by increased hepatic glycogen synthesis and improved glucose tolerance test performance.

MATERIALS AND METHODS

Diabetic mouse models. At weaning, mice (3 wk of age) were placed on either a high-fat diet (59% of calories derived from fat) for diabetic obese mice or a normal chow diet (10% of calories derived from fat) for lean normal mice (Oriental Yeast, Tokyo, Japan) for at least 6 mo. Differences in body weight became significant at 5 wk (Fig. 1*A*). At 6 mo, fasting blood glucose (FBG) levels were increased approximately threefold (Fig. 1*B*) and serum triglycerides by 20% (Fig. 1*C*) in obese diabetic mice relative to lean normal mice.

KKA^{y} mice were purchased from CLEA Japan (Tokyo, Japan) and used for experiments at 10 wk old. All animals were maintained in accordance with the guidelines of the animal experiment committees of Yokohama City University, and experiments were approved by the Ethical Committee of Animal Experiments of Yokohama City University School of Medicine.

Adenovirus construction and injection into mice. Full-length cDNA encoding rat Cav3 was cloned into the shuttle vector to construct an adenoviral vector harboring Cav3 or green fluorescent protein (GFP; control) using an AdenoX adenovirus construction kit (Clontech, Palo

Address for reprint requests and other correspondence: Y. Ishikawa, Cardiovascular Research Institute, Yokohama City University Graduate School of Medicine 3-9 Fukuura, Kanazawa-ku, Yokohama 236-0004, Japan.

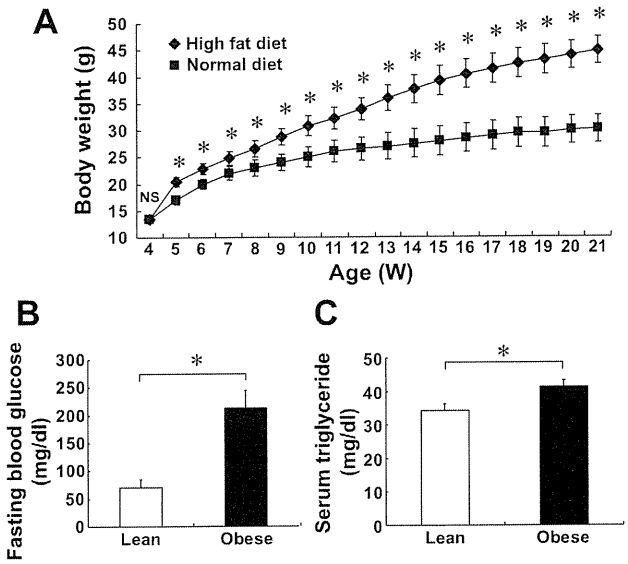

Fig. 1. Generation of obese diabetic mice. *A*: changes in body weight between obese mice and age (W, weeks)-matched, normal lean mice ($n = 31$, $^*P < 0.05$; NS, not significant). *B* and *C*: comparison of fasting blood glucose levels ($n = 8$–13, $^*P < 0.05$) (*B*) and serum triglycerides ($n = 4$–5, $^*P < 0.05$) (*C*) between lean control (Lean) and obese diabetic (Obese) mice.

Alto, CA) (11). An adenovirus titer of 1.0×10^7 plaque-forming units (PFU) was sufficient to overexpress Cav3 in the liver to levels equivalent to endogenous Cav3 in the skeletal muscles, where Cav3 is most abundantly expressed, for up to 6 days after viral injection (Fig. 2, *A* and *B*).

Radioligand binding assays and Western blot analysis. Radioligand binding assays for cell surface IR were performed using HepG2 cells and ^{125}I-labeled insulin as previously described (20, 24). Immunoblotting of Cav, IR-β, and its related molecules was performed as previously described (21, 22).

Immunoprecipitation assays. An in vivo phosphorylation assay for IR-β or insulin receptor substrate (IRS) was performed as previously described (22). After anesthesia was induced with pentobarbital sodium intraperitoneally (100 mg/kg ip), tissues were quickly harvested and stored in liquid nitrogen. Immunoprecipitation of Cav, IR-β, and its related molecules was performed as we previously described (22).

Protein fractionation by the sucrose gradient method. Caveolae fractions were separated by the sodium carbonate-based, detergent-free method (26, 30).

Glucose and insulin tolerance tests. After a 16-h period of fasting, glucose (2 mg/g body wt ip) was injected. FBG levels were determined at 0, 30, 60, 90, and 120 min after injection using a glucometer (22). For the insulin tolerance test, insulin was injected (0.75 U/kg ip), and then FBG levels were measured (7).

Measurements of hepatic glycogen synthesis and triglycerides. Glycogen was measured as previously described (27). Briefly, livers were homogenized in 6 M perchloric acid. The homogenate was boiled for 5 min at 100°C and centrifuged at 10,000 *g*. Glycogen in the supernatant was precipitated with ethanol and measured by a phenol-sulfuric acid reaction. Hepatic triglycerides were extracted as described previously (13). Briefly, tissues were homogenized in extraction buffer (20 mM Tris, pH 7.3, 1 mM EDTA, and 1 mM β-mercaptoethanol), after which chloroform, methanol, and water were added. The mixture was centrifuged at 3,000 *g*. The lower phase was evaporated and redissolved in isopropanol, and triglyceride concentrations were determined with the GPO-Trinder (Sigma, St. Louis, MO).

Measurements of serum lipids. Total cholesterol and triglycerides were determined as we described previously (22).

Cell culture. HepG2 cells, a human hepatocellular carcinoma cell line, were cultured in Dulbecco's modified Eagle's medium containing 5% fetal bovine serum and 10% horse serum in a humidified 95% air-5% CO_2 incubator.

Inhibition of phosphatase activity by Cav peptides. Phosphatase activity was measured colorimetrically using a commercial assay kit (Calbiochem, San Diego, CA) and purified protein tyrosine phosphatase 1B (PTP1B) (Upstate, Lake Placid, NY) in the presence or absence of the following Cav peptides; for the scaffolding domain

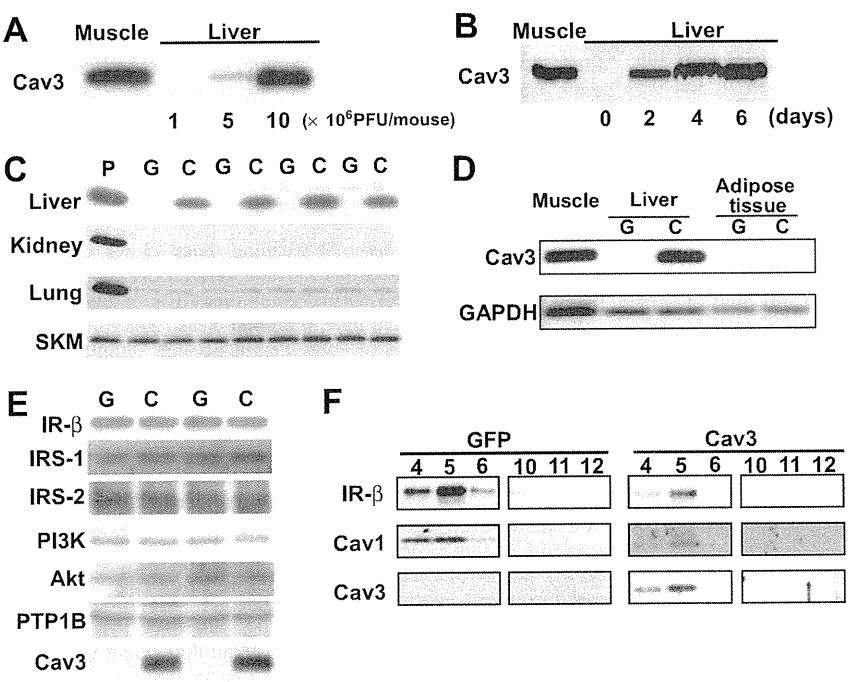

Fig. 2. Caveolin-3 (Cav3) gene transfer to the liver. Adenovirus harboring the Cav3 or green fluorescent protein (GFP) gene was injected into the tail veins of mice. *A*: dose-dependent Cav3 expression in whole liver homogenates. Adenovirus harboring the Cav3 or GFP (control) gene was injected at 0, 1, 5, or 10×10^6 plaque-forming units (PFU). An equivalent amount of total protein from muscle samples was used as positive control (*left lane*). *B*: time-dependent Cav3 expression in the liver. Livers were harvested at 2, 4, and 6 days after injection and analyzed by immunoblotting. *C*: Cav3 expression in various organs of mice after Cav3 gene transfer (C) vs. GFP gene transfer (G). Cav3 protein expression was detected only in the liver. Muscle was used as positive control (P). SKM, skeletal muscle. *D*: Cav3 expression after Cav3 gene transfer in adipose tissues. GAPDH is shown as loading standard. *E*: expression of molecules involved in insulin receptor (IR) signaling in hepatic tissues after Cav3 or GFP gene transfer. IRS-1 and 2, insulin receptor substrate 1 and 2; PTP1B, protein tyrosine phosphatase 1B; PI3K, phosphatidylinositol 3-kinase. *F*: sucrose gradient fractionation of liver proteins and immunoblotting of exogenous Cav3, endogenous Cav1, and IR-β (*lanes 4*, *5*, and *6*, caveolar fractions; *lanes 10*, *11*, and *12*, noncaveolar fractions)

(SD) peptide: Cav3 (SD-Cav3)-DGVWRVSYTTFTVSKYWCYR; Cav1 (SD-Cav1)-DGIWKASFTTFTVTKYWFYR; for the nonscaffolding domain (NSD) peptide: Cav3 (NSD-Cav3)-NRDPKNINEDIVKVDFEDVIAEPEG; Cav1 (NSD-Cav1)-NRDPKHLNDDVVKIDFEDVIAEPEG. Briefly, purified PTP1B (0.022 units) was incubated with increasing concentrations of Cav peptide (0, 0.63, 1.25, 2.5, 5, and 10 μM) at room temperature for 10 min, followed by the addition of the enzyme substrate and an additional 15-min incubation. PTP1B activity was determined by spectrophotometry.

RESULTS

Overexpression of Cav3 in the liver. The liver expressed relatively small amounts of endogenous Cav1, and little Cav3 was detected by immunoblotting mouse liver homogenates. Using the Cav3 adenovirus (1.0×10^7 PFU), Cav3 expression in liver homogenates was comparable to that of endogenous Cav3 in the skeletal muscle (Fig. 2*A*), another major organ involved in regulating glucose metabolism that abundantly expresses Cav. With this amount of adenovirus, the expression of Cav3 peaked at *day 4* postinjection and plateaued at least until *day 6* (Fig. 2*B*). The gene delivery of Cav3 was restricted to the liver, and there was no increase in Cav3 expression in the other organs such as skeletal muscles or adipose tissues (Fig. 2, *C* and *D*). Despite Cav3 overexpression, the protein expression of IR-β as well as other molecules involved in IR signaling such as IRS, phosphatidylinositol 3-kinase (PI3K), Akt, or PTP1B were unchanged (Fig. 2*E*), suggesting that Cav3 does not regulate the protein expression of these molecules, at least, in the liver. The subcellular distribution of exogenous Cav3 and endogenous IR-β, as determined by sucrose gradient fractionation of liver tissues, was unchanged and similar to that of endogenous Cav1 (Fig. 2*F*), and insulin binding assays using intact hepatic cells revealed no changes in B_{max} [GFP vs. Cav3: 4.2 ± 0.1 vs. 4.3 ± 0.2, $n = 4$, P = not significant (NS)] or K_d (GFP vs. Cav3: 58.4 ± 0.1 vs. 58.9 ± 0.4 fmol, $n = 4$, P = NS) with Cav3 gene transfer, suggesting that Cav3 gene transfer did not alter the caveolar and/or the cell surface localization of IR.

Cav3 gene transfer is associated with increased glycogen synthesis in the liver. Because one of the most important actions of insulin is to promote glycogen synthesis in tissues (23), we examined whether Cav3 gene transfer changed the glycogen content in the livers of diabetic obese mice and found that it was significantly increased in mice with Cav3 gene transfer (Fig. 3*A*). Fat deposition was similar in the livers of diabetic obese mice with Cav3 gene transfer and GFP gene transfer, indicating that it was caused by a high-fat diet and not by Cav3 overexpression. The increase in glycogen content in mice with Cav3 gene transfer was accompanied by a decrease in protein expression of the cytosolic form of phosphoenolpyruvate carboxykinase (PEPCK) (Fig. 3*C*). This enzyme catalyzes the first irreversible reaction in gluconeogenesis, and the activity of PEPCK is proportional to the amount of this

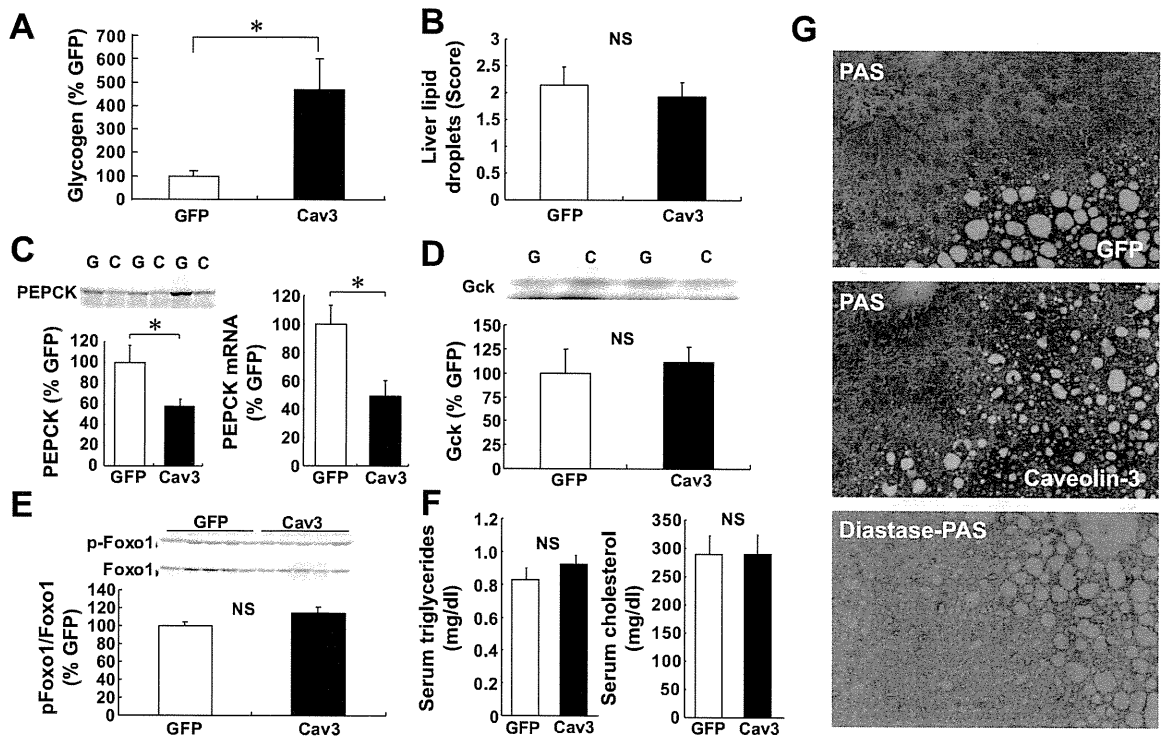

Fig. 3. Increased glycogen content in the liver after Cav gene transfer. *A*: hepatic glycogen content at baseline after Cav3 vs. GFP gene transfer in diabetic obese mice ($n = 4$, $^*P < 0.05$). *B*: hepatic lipid droplet score comparison after Cav3 vs. GFP gene transfer ($n = 7$–8; NS, not significant). *C*: hepatic phosphoenolpyruvate carboxykinase (PEPCK) expression by immunoblotting and quantitative RT-PCR. A representative immunoblot is shown in the *inset* ($n = 4$–5, $^*P < 0.05$). *D*: glucokinase expression by immunoblotting ($n = 4$, NS). *E*: activation of Foxo1 transcriptional factor ($n = 5$, NS). *F*: serum lipid concentrations after Cav3 gene transfer vs. GFP gene transfer in diabetic obese mice (*left*, triglycerides; *right*, cholesterol) ($n = 4$, NS). *G*: histological examination of hepatic tissues. PAS, periodic acid Schiff (PAS) staining of hepatic tissues from mice after Cav3 or GFP gene transfer; diastase-PAS, PAS staining pretreated with diastase.

enzyme, which is regulated by insulin (15). These findings agree with the concept that insulin signals were enhanced in the liver after Cav3 gene transfer. In contrast, the expression of glucokinase (Gck) and Foxo1 activity remained changed (Fig. 3, *D* and *E*).

Abnormal serum lipid concentrations were not improved, potentially because the duration of Cav3 overexpression was short (Fig. 3*F*). Liver triglycerides and serum leptin concentrations were also unchanged (data not shown). Histology and periodic acid-Schiff (PAS) staining demonstrated that the purple staining of glycogen was greater in mice with Cav3 gene transfer (Fig. 3*G*). There was no staining of glycogen when tissues were pretreated with diastase. We also performed oil red O staining and scored the degree of lipid accumulation in hepatic tissues (16). However, there was no significant difference in the lipid score between GFP and Cav3 groups (GFP 1.94 ± 0.34, Cav3 = 2.14 ± 0.25, n = 7–8, P = NS) (Fig. 3*B*).

Similarly, the expression of enzymes involved in lipogenic-related enzymes, such as fatty acid synthase (FAS), sterol regulatory element-binding protein-1, phosphodiesterase 3B, acetyl CoA carboxylase, and liver X receptor, was not significantly different between GFP and Cav3 groups (data not shown).

Cav3 gene transfer improved insulin signals in diabetic obese mice. Cav3 gene injection into diabetic obese mice not only increased the hepatic glycogen content but also improved impaired glucose metabolism. Although Cav3 gene transfer did not alter food intake or body weight (data not shown), impaired glucose tolerance test performance as well as FBG levels (GFP vs. Cav3: 213.3 ± 11.2 vs. 175.3 ± 5.5 mg/dl, n = 8, P < 0.05) were significantly improved (Fig. 4*A*). There was no significant difference in glucose tolerance test performance between non-gene and GFP gene-transferred diabetic obese mice (data not shown). This improvement in glucose metabolism was most likely due to increased insulin action as demonstrated by the improved insulin tolerance test performance (Fig. 4*B*). FBG levels remained lower in mice with Cav3 gene transfer than in control mice with GFP gene transfer, even 90 min after insulin challenge. During the glucose tolerance test, insulin levels were not changed by Cav3 gene transfer (Fig. 4*C*)

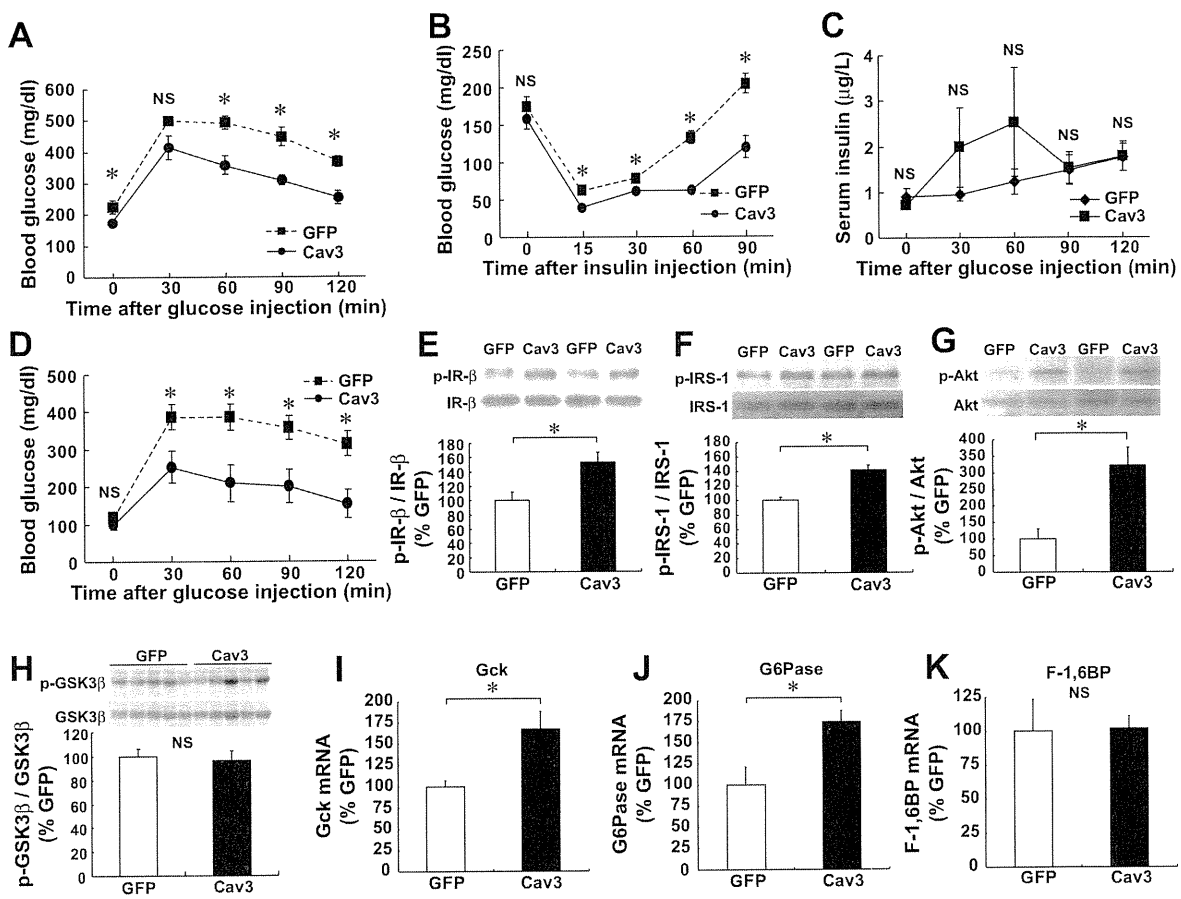

Fig. 4. Cav3 gene transfer improved glucose metabolism in diabetic mice. *A*: glucose tolerance test performance after Cav3 gene transfer and GFP gene transfer in diabetic obese mice (n = 8, *P < 0.05). *B*: insulin tolerance test performance after Cav3 gene transfer vs. GFP gene transfer in diabetic obese mice (n = 4, *P < 0.05). *C*: changes in insulin levels during glucose tolerance test (n = 5, NS). *D*: glucose tolerance test performance in KKA^y mice (n = 4, *P < 0.05). *E–G*: changes in tissue insulin receptor signals after Cav3 gene transfer. Activation of the molecules involved in insulin receptor signaling, IR-β (*E*), IRS-1 (*F*), and Akt (*G*), after Cav3 gene transfer vs. GFP gene transfer in diabetic obese mice. Representative immunoblots are shown in the *insets* (n = 4–5, *P < 0.05). *H*: changes in GSK3β activity (n = 5, NS). *I–K*: mRNA expression of glucose metabolism-related enzyme in mice liver. Glucokinase (Gck; n = 4–5, *P < 0.05), G6Pase (n = 4–5, *P < 0.05), and F-1,6BP (n = 4–5, NS).

KKA^y mice, which have been widely used as a model of Type 2 diabetes (17), showed only a mild increase in fasting blood glucose concentrations (2), but a marked impairment in glucose tolerance test performance. However, when we injected the Cav3 gene into this mouse model, glucose tolerance test performance was significantly improved (Fig. 4*D*). Therefore, the effect of Cav3 gene transfer on insulin signaling occurs in multiple diabetic mouse models.

Changes in hepatic tissue insulin signaling after Cav3 gene transfer. When whole homogenates of livers from diabetic obese mice with Cav3 gene transfer were examined, we found that IR-β, IRS, and Akt phosphorylation was increased (Fig. 4, *E–G*), suggesting that IR signaling increased after Cav3 gene transfer compared with GFP gene transfer. Because the total protein levels of these molecules including IR-β were not increased, this effect was most likely due to the increased activity of IR-β itself. Because Cav3 gene transfer was restricted to the liver, it was also likely that hepatic Cav3 enhanced the response to insulin, leading to an overall improvement in whole body glucose metabolism. We also examined other relevant enzymes such as Gck, G6Pase, and F-1,6BP (Fig. 4, *I–K*). The mRNA expression of Gck and G6Pase were increased in Cav3 group, suggesting transcriptional activation of these enzymes, while that of F-1,6BP was not changed. The activation of GSK3β was not changed either (Fig. 4*H*).

Cav3 overexpression in hepatic cells. A similar enhancement in insulin signaling by Cav was observed in HepG2 cells, a cultured hepatic cell line. Two days after gene transfer, Cav3 was overexpressed in HepG2 cells to levels equivalent to that of endogenous Cav3 in skeletal muscles (data not shown). IR-β and IRS-1 phosphorylation was significantly enhanced at baseline, which was further increased with increasing concentrations of insulin (0–100 nM) (Fig. 5, *A* and *B*). The maximal activation of IRS-1 was significantly greater in Cav3 gene-transferred cells, suggesting that IR kinase activity in response to insulin was increased by Cav3 overexpression, which confirmed our in vivo observations. At high concentrations (>10 nM), IR-β phosphorylation appeared saturated, while IRS-1 activation was further enhanced in a dose-dependent manner. The cellular content of glycogen was also increased at baseline (Fig. 5*C*). We also examined the phosphorylation of insulin-like growth factor receptors (IGF-1R) in mice with Cav3 gene transfer because IR-β and IGF-1R are structurally similar and Cav3 may alter IGF-1R signaling (14). However, the degree of IGF-1R phosphorylation was similar, suggesting that Cav3 specifically enhances IR-β (Fig. 5*D*).

Caveolin-mediated inhibition of PTP1B activity. The activation of other downstream molecules such as extracellular signal-related kinase (ERK) and phosphatase and tensin homolog (PTEN) in the liver was not significantly different between mice that received Cav3 gene transfer and GFP gene transfer (data not shown). In contrast, it is known that phosphatases, such as PTP1B, can also potently regulate the activity of IR signals (8). In addition, previous studies have demonstrated that PTP1B is present in caveolae (22, 30) and physically interacts with Cav (6). We found that the expression of hepatic PTP1B was significantly increased in diabetic obese mice (Fig. 6*A*) and that overexpressed Cav3 coimmunoprecipitated with PTP1B in the liver (Fig. 6*B*). Furthermore, we found that Cav3 inhibited the activity of PTP1B. A SD-Cav3 peptide, which is known to mimic Cav3 (26), inhibited the activity of purified PTP1B in a dose-dependent manner in vitro, while a similar peptide derived from non-SD Cav3 had no effect (Fig. 6*C*). We also found that a peptide from SD-Cav1 similarly inhibited the activity of PTP1B activity while a NSD-Cav1 had no effect (Fig. 6*D*). These results suggest that Cav3 as well as Cav1 directly interacts with and inhibits the activity of PTP1B. Furthermore, this inhibition may be potentiated in the livers of obese mice where PTP1B expression was increased.

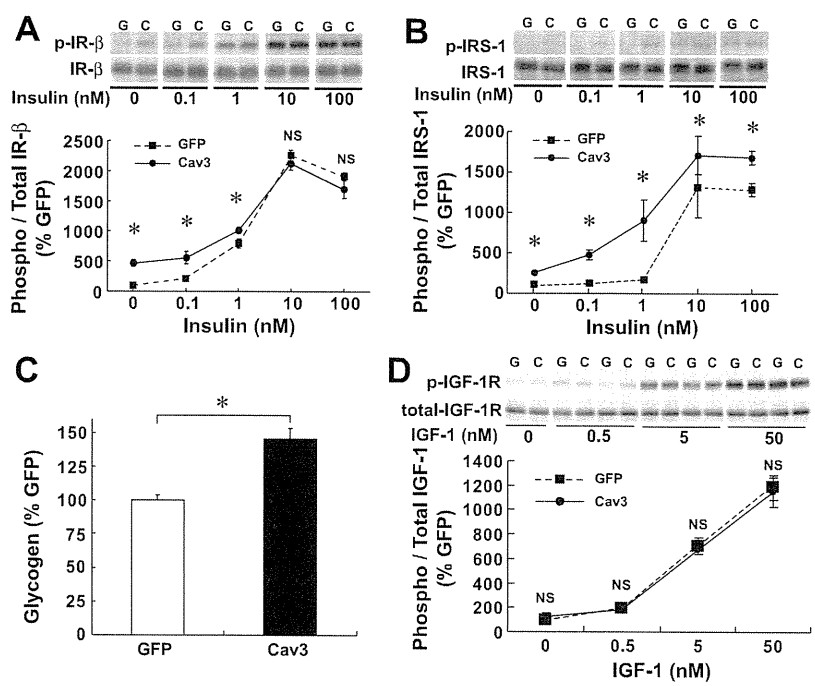

Fig. 5. Cav3 overexpression in HepG2 cells. *A* and *B*: activation of IR-β (*A*) and IRS-1 (*B*) in response to insulin stimulation for 5 min ($n = 5$, $^*P < 0.05$) after Cav3 gene transfer vs. GFP gene transfer. *C*: hepatic glycogen content at baseline after Cav3 gene transfer vs. GFP gene transfer in HepG2 cells ($n = 5$, $^*P < 0.05$). *D*: activation of IGF receptors (IGF-1R) in response to insulin ($n = 4$, NS).

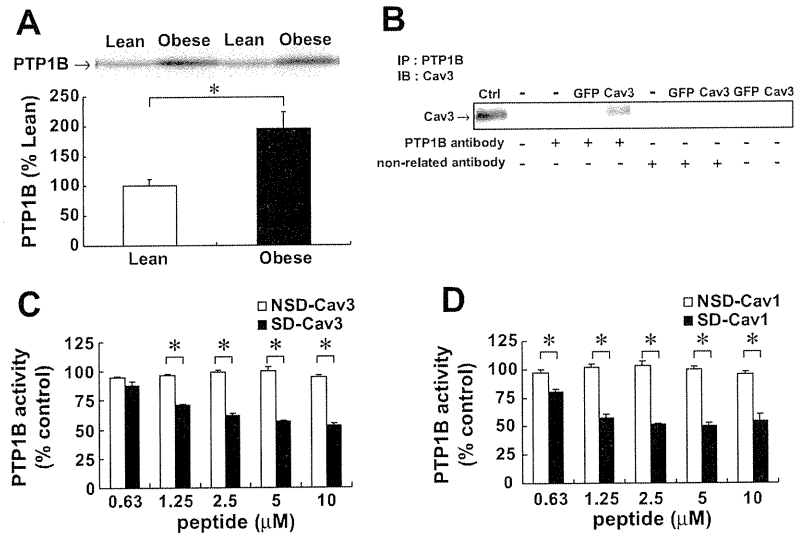

Fig. 6. Caveolin-mediated inhibition of PTP1B activity. *A*: hepatic PTP1B levels by immunoblotting in lean control and obese diabetic mice. A representative immunoblot is also shown ($n = 4$–5, $^*P < 0.05$). *B*: immunoprecipitation assays of PTP1B and Cav3 after Cav3 gene transfer vs. GFP gene transfer in diabetic obese mice. A representative immunoblot is shown. Ctrl, control. *C*: PTP1B activity was determined in the presence of increasing concentrations of scaffolding domain (SD)-Cav3 peptide or nonscaffolding domain (NSD)-Cav3 peptide ($n = 5$, $^*P < 0.05$). *D*: PTP1B activity was determined in the presence of increasing concentrations of SD-Cav1 peptide or NSD-Cav1 peptide ($n = 5$, $^*P < 0.05$).

DISCUSSION

Adenovirus-mediated gene transfer of Cav3 to the liver resulted in increased hepatic glycogen synthesis accompanied by decreased hepatic PEPCK protein levels. Insulin sensitivity, as measured by changes in FBG levels upon insulin injection and glucose tolerance test performance, were improved after Cav3 gene transfer in obese diabetic mice. A similar improvement in glucose metabolism was observed in *KKA*^{y} mice. Overexpression of Cav3 in cultured hepatic cells led to increased phosphorylation of IR-β and IRS in response to insulin stimulation with increased glycogen synthesis at baseline. Therefore, our findings suggest that Cav enhances insulin signals in the liver. The molecular mechanism of this enhanced insulin action may involve direct stimulation of IR by Cav, because a similar mechanism was previously proposed using purified IR and Cav peptides in vitro (30). Although we do not know the extent of caveolin-mediated inhibition of PTP1B activity in vivo, the physical interaction between PTP1B and caveolin has been reported in other studies (6). Furthermore, several investigators have demonstrated the effect of caveolin peptide administration to regulate signaling activity in cells, suggesting that such interaction of caveolin peptide occurs in living cells as well (4, 12, 25, 31).

Furthermore, as shown in the current study, direct inhibition of PTP1B by Cav may be another mechanism by which Cav enhances insulin signals. Obese diabetic mice showed an upregulation of hepatic PTP1B protein, and PTP1B activity was directly inhibited by a SD-Cav3 peptide. Increased expression of phosphatases in obesity was previously reported for other tissues (1). A physical and functional interaction between Cav and PTP1B might be responsible for the slow recovery of glucose levels in insulin tolerance tests as well as for the marked phosphorylation of IR even at low concentrations of insulin (0–1 nM) in mice with Cav3 gene transfer (Fig. 5*A*). Together, Cav3 gene transfer may be a strategy to improve glucose metabolism in vivo.

Adipose and muscle tissues are the major target organs of insulin action that abundantly express Cav1 and Cav3, respectively. Cav may play an important role in these tissues because disruption of the Cav genes, either Cav1 or Cav3, markedly impairs adipose and muscular insulin signals (7, 22). However, the role of Cav in insulin signals in the liver, another major target organ of insulin action, has been uncertain; the liver does not express abundant levels of Cav but has intact insulin signaling. Our findings have demonstrated that Cav can play an important role in insulin signals in the liver, particularly when overexpressed under pathological conditions, such as insulin resistance induced in diabetics by a high-fat diet.

Cav has been long considered a major inhibitor of growth signals and a tumor growth/proliferation suppressor (29), except in prostate cancer (18). Cav gene therapy has been proposed as a potential treatment to suppress tumor proliferation and/or metastasis in various cancers, such as breast cancer (29). Our findings suggest, however, that Cav3 plays an opposite role in insulin signaling; it stimulates IR activity, leading to enhanced IR signals.

In conclusion, Cav3 may be a conditional but important regulator of glucose metabolism. The lack of Cav impaired insulin sensitivity in adipocytes and muscles where endogenous Cav is abundantly expressed (7, 22). Although the liver does not express high levels of Cav under normal conditions, hepatic insulin signals remain intact. However, when insulin signals are impaired in diabetes, increased Cav expression in the liver improves glucose metabolism. The robust nature of our findings suggests that Cav, a membrane-anchoring protein, enhances IR signals.

ACKNOWLEDGMENTS

We thank Masahiro Sakata for technical assistance.

GRANTS

This work was supported in part by grants from the Ministry of Education, Culture, Sports, Science and Technology of Japan and by the Kitsuen Research Foundation.

DISCLOSURES

No conflicts of interest are declared by the author(s).

REFERENCES

1. **Ahmad F, Azevedo JL, Cortright R, Dohm GL, Goldstein BJ.** Alterations in skeletal muscle protein-tyrosine phosphatase activity and expression in insulin-resistant human obesity and diabetes. *J Clin Invest* 100: 449–458, 1997.
2. **Alberts P, Nilsson C, Selen G, Engblom LO, Edling NH, Norling S, Klingstrom G, Larsson C, Forsgren M, Ashkzari M, Nilsson CE, Fiedler M, Bergqvist E, Ohman B, Bjorkstrand E, Abrahmsen LB.** Selective inhibition of 11 beta-hydroxysteroid dehydrogenase type 1 improves hepatic insulin sensitivity in hyperglycemic mice strains. *Endocrinology* 144: 4755–4762, 2003.
3. **Balbis A, Baquiran G, Mounier C, Posner BI.** Effect of insulin on caveolin-enriched membrane domains in rat liver. *J Biol Chem* 279: 39348–39357, 2004.
4. **Bernatchez PN, Bauer PM, Yu J, Prendergast JS, He P, Sessa WC.** Dissecting the molecular control of endothelial NO synthase by caveolin-1 using cell-permeable peptides. *Proc Natl Acad Sci USA* 102: 761–766, 2005.
5. **Carver LA, Schnitzer JE.** Caveolae: mining little caves for new cancer targets. *Nat Rev Cancer* 3: 571–581, 2003.
6. **Caselli A, Mazzinghi B, Camici G, Manao G, Ramponi G.** Some protein tyrosine phosphatases target in part to lipid rafts and interact with caveolin-1. *Biochem Biophys Res Commun* 296: 692–697, 2002.
7. **Cohen AW, Razani B, Wang XB, Combs TP, Williams TM, Scherer PE, Lisanti MP.** Caveolin-1-deficient mice show insulin resistance and defective insulin receptor protein expression in adipose tissue. *Am J Physiol Cell Physiol* 285: C222–C235, 2003.
8. **Elchebly M, Payette P, Michaliszyn E, Cromlish W, Collins S, Loy AL, Normandin D, Cheng A, Himms-Hagen J, Chan CC, Ramachandran C, Gresser MJ, Tremblay ML, Kennedy BP.** Increased insulin sensitivity and obesity resistance in mice lacking the protein tyrosine phosphatase-1B gene. *Science* 283: 1544–1548, 1999.
9. **Galbiati F, Volonte D, Chu JB, Li M, Fine SW, Fu M, Bermudez J, Pedemonte M, Weidenheim KM, Pestell RG, Minetti C, Lisanti MP.** Transgenic overexpression of caveolin-3 in skeletal muscle fibers induces a Duchenne-like muscular dystrophy phenotype. *Proc Natl Acad Sci USA* 97: 9689–9694, 2000.
10. **Gonzalez E, Nagiel A, Lin AJ, Golan DE, Michel T.** Small interfering RNA-mediated down-regulation of caveolin-1 differentially modulates signaling pathways in endothelial cells. *J Biol Chem* 279: 40659–40669, 2004.
11. **Kawabe J, Okumura S, Lee MC, Sadoshima J, Ishikawa Y.** Translocation of caveolin regulates stretch-induced ERK activity in vascular smooth muscle cells. *Am J Physiol Heart Circ Physiol* 286: H1845–H1852, 2004.
12. **Kwiatek AM, Minshall RD, Cool DR, Skidgel RA, Malik AB, Tiruppathi C.** Caveolin-1 regulates store-operated Ca^{2+} influx by binding of its scaffolding domain to transient receptor potential channel-1 in endothelial cells. *Mol Pharmacol* 70: 1174–1183, 2006.
13. **Lampe MA, Burlingame AL, Whitney J, Williams ML, Brown BE, Roitman E, Elias PM.** Human stratum corneum lipids: characterization and regional variations. *J Lipid Res* 24: 120–130, 1983.
14. **LeRoith D, McGuinness M, Shemer J, Stannard B, Lanau F, Faria TN, Kato H, Werner H, Adamo M, Roberts CT Jr.** Insulin-like growth factors. *Biol Signals* 1: 173–181, 1992.
15. **Liu JS, Park EA, Gurney AL, Roesler WJ, Hanson RW.** Cyclic AMP induction of phosphoenolpyruvate carboxykinase (GTP) gene transcription is mediated by multiple promoter elements. *J Biol Chem* 266: 19095–19102, 1991.
16. **Maislos M, Medvedovskv V, Sztarkier I, Yaari A, Sikuler E.** *Psammomys obesus* (sand rat), a new animal model of non-alcoholic fatty liver disease. *Diabetes Res Clin Pract* 72: 1–5, 2006.
17. **Mauldin JP, Srinivasan S, Mulya A, Gebre A, Parks JS, Daugherty A, Hedrick CC.** Reduction in ABCG1 in Type 2 diabetic mice increases macrophage foam cell formation. *J Biol Chem* 281: 21216–21224, 2006.
18. **Mouraviev V, Li L, Tahir SA, Yang G, Timme TM, Goltsov A, Ren C, Satoh T, Wheeler TM, Ittmann MM, Miles BJ, Amato RJ, Kadmon D, Thompson TC.** The role of caveolin-1 in androgen insensitive prostate cancer. *J Urol* 168: 1589–1596, 2002.
19. **Oka N, Yamamoto M, Schwencke C, Kawabe J, Ebina T, Couet J, Lisanti MP, Ishikawa Y.** Caveolin interaction with protein kinase C: isoenzyme-dependant regulation of kinase activity by the caveolin scaffolding domain peptide. *J Biol Chem* 272: 33416–33421, 1997.
20. **Okumura S, Kawabe J, Yatani A, Takagi G, Lee MC, Hong C, Liu J, Takagi I, Sadoshima J, Vatner DE, Vatner SF, Ishikawa Y.** Type 5 adenylyl cyclase disruption alters not only sympathetic but also parasympathetic and calcium-mediated cardiac regulation. *Circ Res* 93: 364–371, 2003.
21. **Okumura S, Vatner DE, Kurotani R, Bai Y, Gao S, Yuan Z, Iwatsubo K, Ulucan C, Kawabe J, Ghosh K, Vatner SF, Ishikawa Y.** Disruption of type 5 adenylyl cyclase enhances desensitization of cyclic adenosine monophosphate signal and increases Akt signal with chronic catecholamine stress. *Circulation* 116: 1776–1783, 2007.
22. **Oshikawa J, Otsu K, Toya Y, Tsunematsu T, Hankins R, Kawabe J, Minamisawa S, Umemura S, Hagiwara Y, Ishikawa Y.** Insulin resistance in skeletal muscles of caveolin-3-null mice. *Proc Natl Acad Sci USA* 101: 12670–12675, 2004.
23. **Quinn PG.** Inhibition by insulin of protein kinase A-induced transcription of the phosphoenolpyruvate carboxykinase gene. Mediation by the activation domain of cAMP response element-binding protein (CREB) and factors bound to the TATA box. *J Biol Chem* 269: 14375–14378, 1994.
24. **Shiraishi S, Yamamoto R, Yanagita T, Yokoo H, Kobayashi H, Uezono Y, Wada A.** Down-regulation of cell surface insulin receptors by sarco(endo)plasmic reticulum Ca^{2+}-ATPase inhibitor in adrenal chromaffin cells. *Brain Res* 898: 152–157, 2001.
25. **Sukumaran SK, Quon MJ, Prasadarao NV.** *Escherichia coli* K1 internalization via caveolae requires caveolin-1 and protein kinase Calpha interaction in human brain microvascular endothelial cells. *J Biol Chem* 277: 50716–50724, 2002.
26. **Toya Y, Schwencke C, Couet J, Lisanti MP, Ishikawa Y.** Inhibition of adenylyl cyclase by caveolin peptides. *Endocrinology* 139: 2025–2031, 1998.
27. **Varagic VM, Mrsulja BB, Stosic N, Pasic M, Terzic M.** The glycogenolytic and hypertensive effect of physostigmine in the anti-nerve-growth-factor-serum-treated rats. *Eur J Pharmacol* 12: 194–202, 1970.
28. **Williams TM, Cheung MW, Park DS, Razani B, Cohen AW, Muller WJ, Di Vizio D, Chopra NG, Pestell RG, Lisanti MP.** Loss of caveolin-1 gene expression accelerates the development of dysplastic mammary lesions in tumor-prone transgenic mice. *Mol Biol Cell* 14: 1027–1042, 2003.
29. **Williams TM, Lisanti MP.** Caveolin-1 in oncogenic transformation, cancer, and metastasis. *Am J Physiol Cell Physiol* 288: C494–C506, 2005.
30. **Yamamoto M, Toya Y, Schwencke C, Lisanti MP, Myers MG Jr, Ishikawa Y.** Caveolin is an activator of insulin receptor signaling. *J Biol Chem* 273: 26962–26968, 1998.
31. **Zhu L, Schwegler-Berry D, Castranova V, He P.** Internalization of caveolin-1 scaffolding domain facilitated by Antennapedia homeodomain attenuates PAF-induced increase in microvessel permeability. *Am J Physiol Heart Circ Physiol* 286: H195–H201, 2004.